Evolutionary dynamics of nascent multicellular lineages

Guilhem Doulcier[1, 2, 3, *,✉], **Philippe Remigi**[4, 5, *,✉], **Daniel Rexin**[4, 6, 7 *,✉], **and Paul B. Rainey**[4, 3, 6,✉]

[1]Philosophy Department, Macquarie University, Sydney, New South Wales 2109, Australia
[2]Department of Theoretical Biology, Max Planck Institute for Evolutionary Biology, Plön, Germany
[3]Laboratory of Biophysics and Evolution, ESPCI, Université Paris Sciences et Lettres, Paris, France
[4]New Zealand Institute for Advanced Study, Auckland, New Zealand
[5]Laboratoire des Interactions Plantes-Microbes Environnement (LIPME), INRAE, CNRS, Université de Toulouse, Castanet-Tolosan, France
[6]Department of Microbial Population Biology, Max Planck Institute for Evolutionary Biology, Plön, Germany
[7]Institute of Environmental Science and Research Ltd., ESR, Porirua, New Zealand
[*]Co-first authors

The evolution of multicellular organisms involves the emergence of cellular collectives that eventually become units of selection in their own right. The process can be facilitated by ecological conditions that impose heritable variance in fitness on nascent collectives with long-term persistence depending on capacity of competing lineages to transition reliably between soma- and germ-like stages of proto-life cycles. Prior work with experimental bacterial populations showed rapid increases in collective-level fitness with capacity to switch between life cycle phases being a particular focus of selection. Here we report experiments in which the most successful lineage from the earlier study was further propagated for 10 life cycle generations under regimes that required different investment in the soma-like phase. To explore the adaptive significance of switching, a control was included in which reliable transitioning between life cycle phases was abolished. The switch proved central to maintenance of fitness. Moreover, in a non-switch treatment, where solutions to producing a robust and enduring soma-phase were required, evolution of *mutL*-dependent switching emerged *de novo*. A newly developed computational pipeline (`colgen`) was used to display the moment-by-moment evolutionary dynamics of lineages providing rare visual evidence of the roles of chance, history and selection. `Colgen`, underpinned by a Bayesian model, was further used to propagate hundreds of mutations back through temporal genealogical series, predict lineages and time points corresponding to changes of likely adaptive significance, and in one instance, via a combination of targeted sequencing, genetics and analyses of fitness consequences, adaptive significance of a single mutation was demonstrated. Overall, our results shed light on the mechanisms by which collectives adapt to new selective challenges and demonstrate the value of genealogy-centered approaches for investigating the dynamics of lineage-level selection.

Experimental evolution | Bayesian Network | Genealogies | Evolutionary transitions in individuality | Ecological Scaffolding | Multicellularity | Metapopulations

Correspondence:
guilhem.doulcier@normalesup.org (GD)
philippe.remigi@inrae.fr (PR)
daniel.rexin@gmail.com (DR)
rainey@evolbio.mpg.de (PBR)

Introduction

Major evolutionary transitions in individuality underpin the emergence of life's complexity (Buss, 1987; Maynard Smith and Szathmary, 1995; Michod, 2000; Okasha, 2006). A transition of particular interest is that involving the formation of multicellular collectives from ancestral unicellular types (Bonner, 1998; Grosberg and Strathmann, 2007; Herron et al., 2022; Rainey and De Monte, 2014). The transition initiates with the formation of simple groups – for example, through failure of cells to separate upon cell division – and completes once groups become units of selection in their own right. For the latter, newly formed collectives must be Darwinian, that is, collectives must be discrete (with variation among collectives), replicate, and leave offspring copies that resemble parental types (Godfrey-Smith, 2009).

As elaborated elsewhere, these Darwinian properties are derived traits and require evolutionary explanation (Griesemer, 2001; Rainey and Kerr, 2010). But how these properties evolve – in the absence of collectives already manifesting these properties – has been a puzzle. One solution that has motivated experimental studies recognises that variation, replication and heredity can be exogenously imposed (scaffolded) by specific ecological conditions (Black et al., 2020; Bourrat, 2022; Doulcier et al., 2020, 2023; Rainey et al., 2017). Once stably imposed, simple undifferentiated groups of cells can become unwitting players in a selective process that occurs over timescales defined by the birth and death of groups, just as if they were cells of a multicellular organism.

A conceivable ecological setting – and one that has inspired laboratory studies – is provided by reeds in a pond (Rainey et al., 2017). Reeds act as scaffolds around which microbial mats attach allowing colonisation of the air-liquid interface (ALI), but importantly spatial separation of reeds ensures that mats are discrete, thus allowing variation to manifest at the level of mats. Periodically mats fail and sink, opening niches for formation of new mats. If dispersing cells from an extant mat re-colonise a vacant reed, then the newly formed mat, being derived from the extant parent, may inherit parental characteristics. Mats thus become units of selection in their own right with selection operating over two timescales: the doubling time of mats, and the doubling time of cells (Black et al., 2020). Knowledge of the evolutionary dynamics that unfold at the level of mats stand to shed light on processes underpinning the origin of multicellular life.

In the laboratory, an analogy of the reeds-in-pond model

has been devised by substituting glass vials for reeds with experimental realisation in earlier studies (Hammerschmidt et al., 2014; Rose et al., 2020). In brief, the work uses the aerobic bacterium *Pseudomonas fluorescens* SBW25, whose metabolic activities, when introduced into static broth microcosms, causes the medium to become anoxic (Koza et al., 2011). This creates conditions that favour cellulose-over-producing, ALI-colonising (mat-forming) mutants known as "wrinkly spreaders" (WS). Presence at the ALI ensures that constituent cells benefit from freely available oxygen. Given a cost associated with the over-production of cellulose, WS mats are susceptible to invasion by cellulose defective "smooth" (SM) mutants. These types pay none of the costs, but fail to provide structural support to the mat, ultimately lead to mat collapse (Rainey and Rainey, 2003). While this amounts to a classic tragedy of the commons (Hardin, 1968), taken back into the pond setting, functional roles of WS mat-forming cells and swimming SM cells can be viewed as analogous to primitive soma and germ phases, respectively (Rainey and Kerr, 2010). WS mats perform an ecological role (ensuring access to oxygen) while producing seeds (SM cells) of the next generation of mats. The latter is especially relevant because in the absence of propagules, mats, like soma, are an evolutionary dead-end (Hammerschmidt et al., 2014).

A graphical representation of both the life cycle and the lineage selection regime is provided in Figure 1. Negative frequency dependent interaction among WS and SM cells generates a life cycle that in appropriate ecological context becomes the primary focus of selection. Important to note are the causes of lineage-level death-birth dynamics. Lineages go extinct whenever they fail to generate the next stage in the life cycle, or because the mat phase collapses prematurely (soma failure). Given that the life cycle is fuelled by spontaneous mutation, lineages are particularly prone to failure, with lineage death providing opportunity for extant lineages (chosen at random) to export their reproductive success to new microcosms in precisely the same way as a mat that falls from a reed provides opportunity for competing mats to reproduce.

The experiment originally conducted by Hammerschmidt et al. (2014) was performed over 10 life cycle generations with selection rewarding lineages that repeatedly transitioned through soma and germ phases. On conclusion of the experiment a single lineage (Line 17) had swept to fixation. Detailed analysis showed that success was a consequence of collective-level benefits arising from a simple genetic switch. Of a numerous array of mutations, two were of special significance: one that caused the WspR digualnylate cyclase (DGC) to achieve a state of constitutive activation (thus over-producing c-di-GMP and eliciting over-production of cellulose), and a second, loss-of-function mutation, in *mutS* (A1489C), a gene involved in methyl-directed mismatch repair. The latter, while causing an overall elevation in mutation rate, specifically increases frame-shifting in tracts of guanine (G) residues (Heilbron et al., 2014). While tracts of Gs are rarely found in any genome, one – composed of seven G residues – happens to reside in the active site of the DGC domain of WspR. Given the defect in *mutS*, WspR gained ability to switch rapidly between functional and non functional states (due to elevated rates of frame-shifting), thus ensuring reliable transitions between soma and germ phases (Hammerschmidt et al., 2014).

Here we took the adaptive genotype and an isogenic lineage in which the genetic switch was rendered inoperable and asked whether the genetic switch delivers longer-term evolutionary advantage. We also explored the extent to which the switch facilitates lineage-level responses to the challenge of growing in larger diameter microcosms requiring substantially greater investment in the soma phase. Underpinning our analyses is `colgen`, a newly developed analytical tool that provides graphical representation of genealogies, a variety of means for exploring lineage dynamics, and, supported by a Bayesian model, allows inferences as to branch points of likely adaptive significance. Further, when combined with DNA sequence from derived lineages `colgen` predicts the sequence of causal mutational events. Subsequent genetic analyses support the value of these predictions.

Material and Methods

Experimental evolution of collectives.

The experimental protocol is as described previously Hammerschmidt et al. (2014) and depicted in Figure 1a-c. The two genotypes used here, Line 17 (hereafter Life Cycle Switch +, LCS^+) and the isogenic variant in which the *mutS* A1489C was reverted to wild type (hereafter Life Cycle Switch -, LCS^-), are derived from Hammerschmidt et al. (2014).

Both LCS^+ and LCS^- genotypes were propagated through 10 life cycle generations in standard (S) 17 mm diameter microcosms, and in parallel, in large (L) microcosms of 35 mm diameter, with respectively 9.5 and 31.5 ml media to keep surface area to volume ratio constant. Two genotypes, multiplied by two sizes of microcosm, results in four experimental regimes, designated S-LCS^+, L-LCS^+, S-LCS^-, L-LCS^-.

Ten life cycle generations were performed on 48 parallel cultures blocked as six meta-populations of eight lineages. As in the reeds-in-pond thought experiment, lineages that fail to complete the life cycle and go extinct provide opportunity for viable collective lineages to reproduce. Upon demise of a lineage, a viable type from the same block is chosen at random and allowed to replace the extinct type. In the case where all cultures from a given block become extinct at the same time, random cultures from viable blocks are used to replace the extinct lineages.

Measuring lineage-level fitness.

Previously measures of fitness have involved lineage-level competition experiments against ancestral types that are often difficult to interpret and challenging to conduct (Hammerschmidt et al., 2014). Observation of the genealogies of lineages as shown in Figure 3 led to realisation that the probability of avoiding extinction is a good predictor of future evolutionary success (Palmer and Feldman, 2012). Hence-

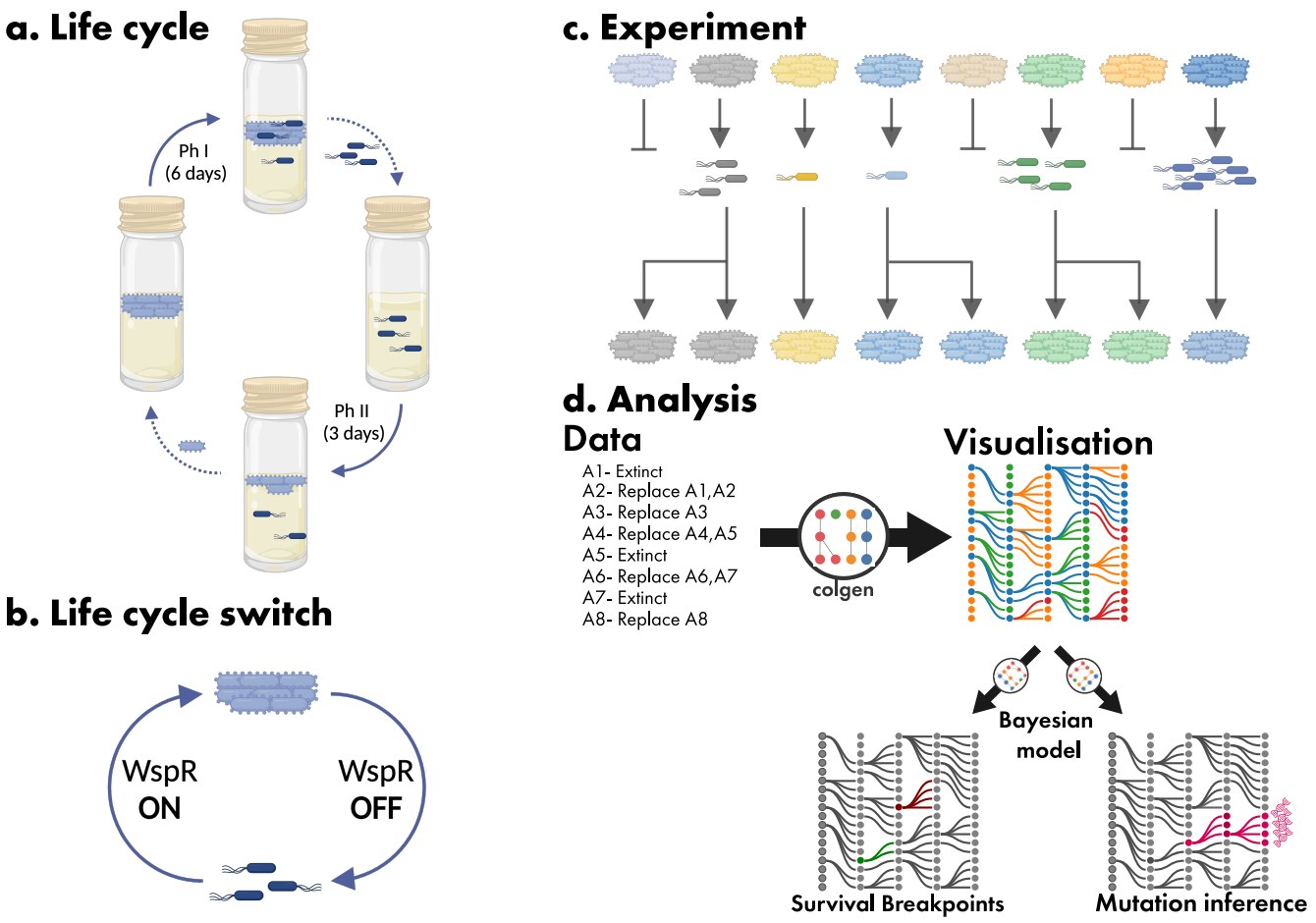

Figure 1. Experimental regime and `colgen`-based representation. **a** A single generation of the nascent multicellular life cycle has two phases. Phase I (Ph I) initiates with placement of a single WS genotype into a glass microcosm. The WS type over-produces cellulose and forms a soma-like structure (a mat) at the air-liquid interface (ALI). During the six day Ph I stage the mat, in addition to remaining at the ALI, must generate non-cellulose producing (SM) cells that function as seeds (germ cells) for the next generation of mats (solid arrow). At the end of Ph I, SM germ cells are transferred to a fresh microcosm (dotted arrow) where the soma state must be re-established. After three days in Phase II (Ph II) WS cells are collected and a single genotype used to found the next generation. **b** Transition between soma (WS) and germ (SM) states involves activating and deactivating production of cellulose, which is effected by mutations that activate and deactivate the synthesis of cyclic-di-GMP. Of particular relevance is the derived "life cycle switch" LCS$^+$ genotype that has enhanced capacity to transition between soma and germ states because of a mutation in *mutS* that causes frameshifting to occur at high frequency in a tract of guanine (G) residues in the active site of the WspR-encoded diguanylate cyclase. When the reading frame is intact, the cellulose-overproducing soma state is acheived, but gain or loss a G-residue causes a frameshift, deactivation of WspR and realisation of the germ state. **c** Extinction of lineages occurs if there are no soma cells after six days of Ph I, no germ cells after three days in Ph II, or if the mat collapses during Ph I (soma failure). Death of lineages allows a death-birth dynamic to unfold with lineages functioning as units of selection in their own right. A single meta-population of eight distinct lineages is shown. While lineages compete, then never mix. Extant lineages replace themselves, but also have the possibility of reproducing on death of a competing lineage. Selection rewards persistence which depends on reliable transitioning between states. **d** Schematic description of three functions of the `colgen` package: visualisation (Section A), survival breakpoint detection (Section B) and belief propagation (Section C).

forth, measures of fitness were determined, not by competition with an ancestral type, but by measuring the number of lineage extinction events after replicate lineages of single test genotypes have gone through a further life cycle generation. Further details are available in Supplementary note 3.

Sequencing.

All WS genotypes chosen at the end of generation 10 – in lieu of founding generation 11 – were subject to whole genome sequencing. Bacterial genomic DNA was extracted from static overnight cultures of WS clones using the Wizard Genomic DNA purification kit (**A1125**, Promega) following the manufacturer's instructions. Whole genome sequencing was performed using Illumina sequencing technology. Short reads were mapped on the *Pseudomonas fluorescens* SBW25 reference genome (GCF000009225_2) and mutations were identified with Breseq v. 0.32.1 (Deatherage and Barrick, 2014) using default parameters. When taking into account extinctions within cycle 10 and filtering out sequence data of poor quality, 45 of 48 endpoint genotypes were sequenced for L-LCS$^+$, 48 of 48 for S-LCS$^+$ 42 of 48 for L-LCS$^-$ and 37 of 48 for S-LCS$^-$. Further genotypes were targeted for sequencing using the same protocol after the experiment concluded, based on analysis of genealogies. In S-LCS$^+$, genotypes at each cycle, in L-LCS$^+$ 1-II-A7 (cycle 1, Ph II, lineage A7) 2-I-A5, 2-II-A6, 2-II-A7, 2-II-A8, 3-II-A1 and 3-II-E2 were sequenced in order to elucidate the origin of the *mutL* mutation. Further details are available in Supplementary note 2.

Analysis of collective genealogies using the `colgen` package.

Each new cycle of the experiment produced a set of complex data: for each lineage, the record of germ and soma-like cell census, the presence of the soma state, and additionally death-birth events, were recorded. Plotting and visualisation features of `colgen` (Doulcier, 2019, v 2.0b1) were used to synthesise data without discounting complexity. Survival probability, as determined via `colgen` (Section B, described in Supplementary note 1) was combined with DNA-sequence information to identify genotypes of likely adaptive significance (Section C (described in Supplementary note 2).

All results obtained using `colgen` in the context of this manuscript can be explored interactively online: https://doi.org/10.5281/zenodo.11170876.

Results

The experimental regime is as depicted in Figure 1a-c and was performed as previously described (Hammerschmidt et al., 2014; Rose et al., 2020), but with two differences: the first, concerns the founding genotypes, and the second, inclusion of larger diameter microcosms. The founding genotypes are derived from the study of Hammerschmidt et al. (2014): one, referred to in that study as "Line 17", and hereafter as the "life cycle switch" (LCS$^+$) type; the other, the LCS$^-$ type that differs from LCS$^+$ by a single mutation that renders the life cycle switch inoperable (reversion of *mutS* to the ancestral functional state (C1489A)). The inclusion of large (as well as standard size) microcosms provided a new selective challenge requiring evolving lineages to find solutions to building a significantly more substantial soma (mat) phase. The combination of two genotypes (LCS$^+$ and LCS$^-$) plus two environments (standard (S) and large (L) microcosms) delivers four treatments: S-LCS$^+$, L-LCS$^+$, S-LCS$^-$ and L-LCS$^-$. Each treatment was composed of 48 microcosms blocked as six metapopulations (A-F) of eight lineages. All were propagated for 10 life cycle generations (see Materials and Methods and Figure 1 for further information).

A. Eco-evolutionary dynamics.

Figure 2 shows the frequency of lineage extinctions and their causes. Extant lineages are in blue, with extinctions due failure to produce germ cells shown in red, failure of the soma phase (mat) in orange, and failure to produce soma cells in green (see figure caption). LCS$^+$ treatments showed little change (S-LCS$^+$ even less than L-LCS$^+$), which indicates that these lineages are close to an evolutionary equilibrium. In contrast, the proportion of lineages that survived in the LCS$^-$ treatments was initially low, but rapidly increased. Figure S1 shows the proportion of lineages that avoided extinction at each of the 10 life cycle generations. It also reveals how changes in survival during one phase correlates with changes in survival during the other. Viewed as displayed in Figure S1, and comparing the first and the tenth generations, the data indicate for all, but L-LCS$^-$, a trade-off between survival in Ph I versus Ph II.

Data presented in Figure 2 averages the proportion of collectives that avoid extinction across the entire population of lineages at each time point. It masks heterogeneity, including the fact that some lineages are evolutionary dead-ends, while others rise to fixation. A more information-rich representation is one where the evolutionary fate of each lineage is displayed along with the causes of extinction.

Figure 3 provides such a visual representation. Immediately apparent are treatment-specific differences in lineage dynamics, with those founded by LCS$^+$ suffering fewer extinction events compared to those founded by LCS$^-$. This is true for both continued selection in standard size microcosms and in the face of challenges posed by evolving in large diameter microcosms. Where improvement is evident, it is most apparent in the capacity of lineages to form mats able to endure the entire six-day period of Ph I. Interestingly this trend is reversed in S-LCS$^+$ where death due to mat failure increased during course of the experiment. Production of the germ-line phase during Ph I and soma-phase during Ph II posed greatest challenge to LCS$^-$ treatments, but also showed improvement during the course of the experiment.

Examination of the coalescent tree(s) (depicted in solid colour) reveals further differences among treatments. LCS$^+$ maintained in standard microcosms showed few deaths with half of the founding lineages remaining intact at the end of the experiment. On the other hand, LCS$^-$ lineages propagated in large microcosms narrowly escaped extinction, with extant lineages, on conclusion of the experiment, being descendants of just a single ancestral microcosm (microcosm 2-II-A5 — generation 2, Ph II, microcosm A5).

As is typical of selection experiments, measures of fitness of derived types, relative to ancestral types, provides an overall measure of the response to selection. Previously, such measures have involved lineage-level competition experiments that are difficult to interpret and challenging to conduct Hammerschmidt et al. (2014); Rose et al. (2020). Observation of the genealogies of lineages Figure 3 led to realisation that the probability of avoiding extinction is a sound predictor of future evolutionary success. Henceforth, measures of fitness were determined, not by competition with an ancestral type, but by measuring the number of lineage extinction events after replicate lineages (of single test genotypes) were cycled through a further generation (Supplementary note 3).

The data, shown in Figures S17 to S20, is largely concordant with that shown in Figure 2. LCS$^+$ lineages evolving in standard microcosms showed overall a decline in fitness relative to the ancestral type (Figure S17a) with negative contributions coming from both reductions in durability of the soma phase (Figure S17b) and in capacity to switch between life cycle phases (Figure S17c-d). This negative trend was not apparent for LCS$^+$ types in large microcosms, where the fitness of all derived lineages exceed the ancestral type (Figure S18a).

The fitness of derived LCS$^-$ lineages in standard microcosms was highly variable, with some test genotypes having elevated fitness, but others with reduced fitness. Low

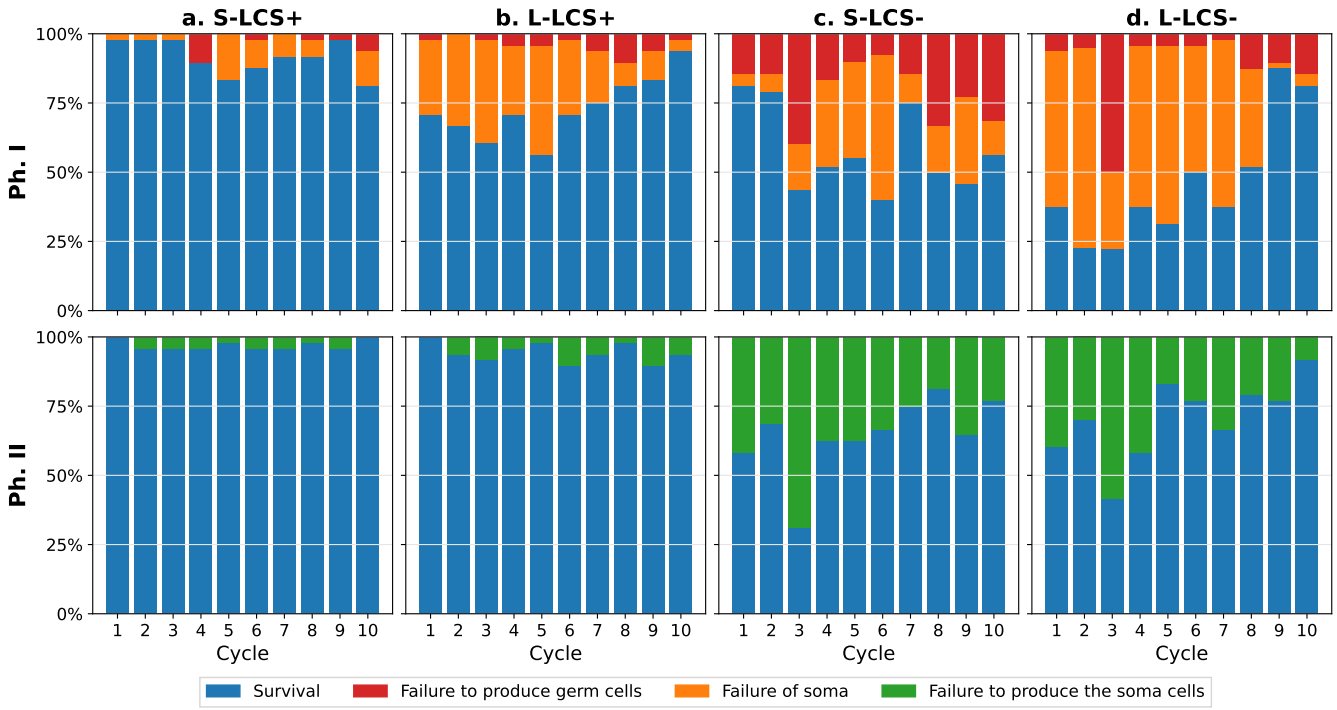

Figure 2. Proportion of surviving collectives in phase 1 and 2 for each cycle. The stacked bar correspond to the proportion of surviving collective for each cycle. Blue denotes extant lineages, with red, orange and green marking extinct lineages and causes of extinction: during Ph I, failure to produce the germ cells (red), failure of the mat to remain intact for the required six days (orange), and during Ph II, failure to produce soma cells (green). Each column is different treatment, LCS$^+$: Lineage 17 from Hammerschmidt et al. (2014) with a life cycle switch, LCS$^-$: same lineage with the switch reverted, S: standard microcosms, L: large microcosms.

probability of switching was the primary cause of low fitness (Figure S19cd). This is understandable in terms of the availability of mutational routes for switching between soma and germ phases becoming increasingly limited as a consequence of prior mutational cycles. In contrast, in large microcosms, there was a noticeable improvement in fitness of all tested LCS$^-$ lineages (Figure S20a), primarily in terms of ability to produce an enduring soma phase (Figure S20b).

B. Identifying likely adaptive events.

The genealogical connections depicted in Figure 3 show what appear to be selective sweeps. Those microcosms that mark the start of such sweeps indicate points at which adaptive mutations may have arisen. However, as the number of offspring at any time-point is dependent on death of competing lineages, the connection to adaptive potential can be difficult to infer. For example, it is not inconceivable that a poorly performing, but nonetheless extant, lineage happens to amplify, not because of improvements in fitness, but by chance. To distinguish improvements in future representation due to chance versus selection, a measure of enduring "adaptive potential" associated with each node is desirable.

To this end, we employed a Bayesian network model in conjunction with an evidence-propagation algorithm (Koller and Friedman, 2009) to predict improvement in the probability of survival. The model assumes existence of a hidden *probability of survival* value for each node, which is calculated by computing the maximum-a-posteriori value, using an expectation-maximisation algorithm that takes genealogical data and transmission model as input. Details of the procedure are described in Supplementary note 1. Nodes associated with marked improvement stand as indicators of time points at which mutations predicted to have adaptive significance occurred. While we bring particular focus to the L-LCS$^-$ treatment, identical analyses were performed on the remaining three treatments and are reported in Figure S2.

Figure 4 shows the result of the analysis for the L-LCS$^-$ treatment. According to the maximum-*a-posteriori* procedure, genotypes that are ancestors of lineages where the probability of survival markedly improved are 2-I-A3 (generation 2, Ph I, lineage A3; marked A3 on the figure), as well as 1-II-A7, 2-II-A5, 3-I-A5, 3-II-E2, 4-I-E2 and 5-I-E3. Note that all these lineages had extant descendants at the end of the experiment. Moreover, 1-I-F8, 1-II-A7, 2-I-A3 and 2-II-A5 are ancestral to the entire population of lineages at generation 10.

In the next section, we describe how mutational data derived from whole genome sequencing – primarily of derived lines at generation 10 – aid elucidation of the genetic bases of fitness improvements.

C. Propagating mutational data to the full genealogy.

Whole genome sequence was obtained from all single WS (soma) genotypes derived from each extant lineage at the end of generation 10 (see Figure S8 for details), and from the single WS genotypes derived from the six selected microcosms marked in Figure 4. DNA sequence reads were aligned to the ancestral SBW25 genome leading to identification of a total of 3,686 mutations (across all four treatments). Because the 10 generations reported here were derived from LCS$^+$, which had already experienced 10 prior generations of evolution,

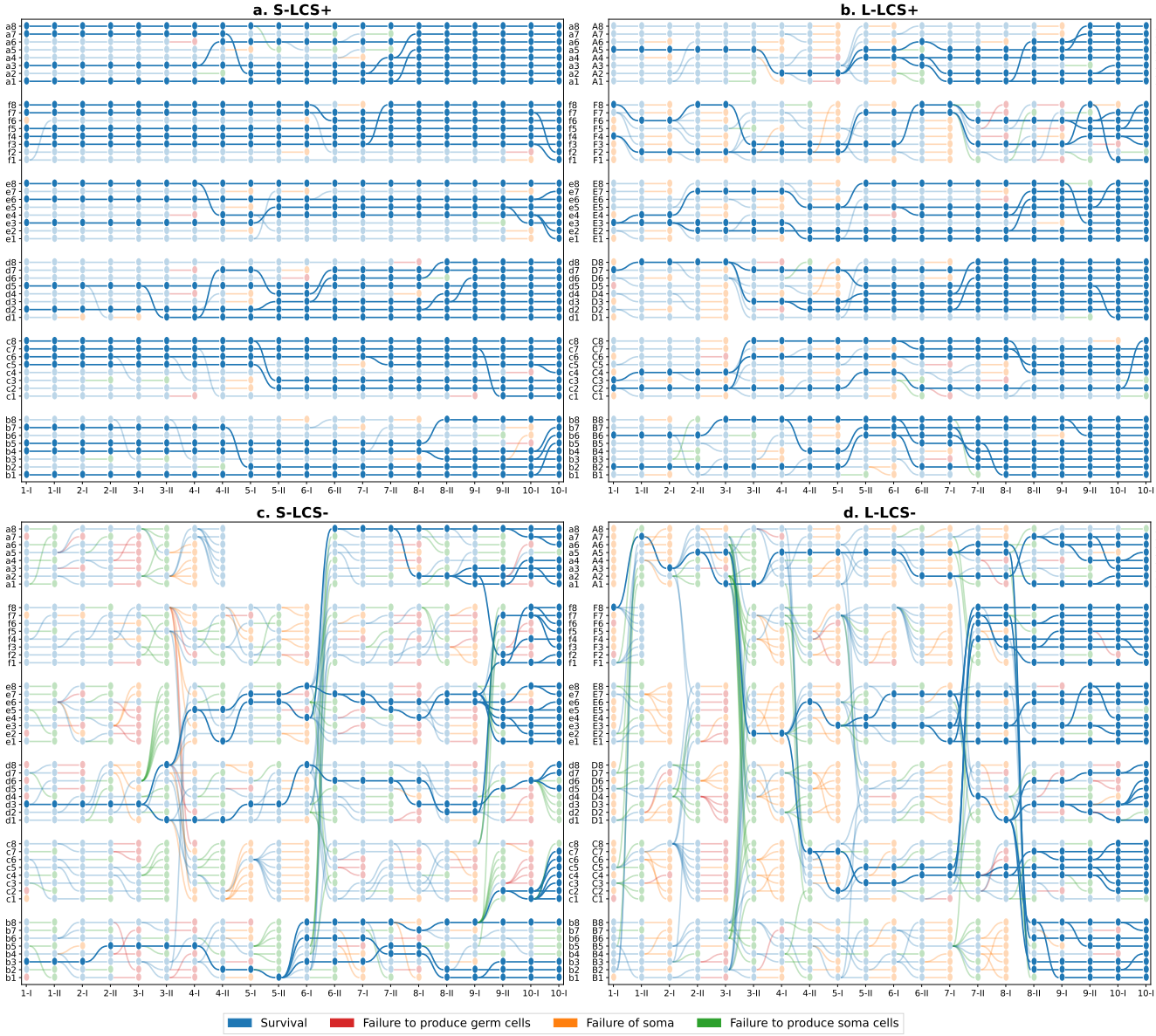

Figure 3. Lineage genealogies. The lineage-level selection experiment yields a rich data set of 48 parallel microcosms (lineages) for each treatment with associated extinction (colours) and replacement events (edges). Lineage-level genealogies in the shape of directed acyclic graphs offer a synthetic but more granular visualisation compared to the proportion of events at each phase (Figure 2). The x-axis labels are phases within each life cycle generation, with 1-I indicating the end of Ph I of the first cycle, 1-II, the end of Ph II of the first cycle and so forth. The gaps (L-LCS$^+$ population F in 2-I, 2-II, 3-I and S-LCS$^-$ population a in 5-I, 5-II, 6-I) are missing due to technical errors.

we removed those mutations (58 in total) that accrued during the previous experiment. The full data set is available at XXX. While this represents an overwhelming number of mutations, in part, expected, because of the mutator status of the LCS$^+$ genotype, mapping of mutations on genealogies is nonetheless possible. A belief-propagation algorithm similar to that described in the previous section was used. This builds upon the fact that an identical mutation found in two or more descendant lineages most likely emerged in a single ancestral lineage whose identity can be inferred from patterns of genealogical connections. The procedure is detailed in Supplementary note 2.

Given the large number of mutations, analysis began by firstly propagating the mutations from the end point (combined with additional information from the six focal lineages from L-LCS$^-$) backward through each genealogy. The results, shown in Figure 5, reveal that lineages evolving under the S-LCS$^-$ treatment (represented by dots) accumulated few mutations during the course of the experiment. This is as expected given that a single mutation underpins the transition between each phase of the life cycle: two mutations per cycle and thus ≈ 20 over the course of 10 generations. In contrast, lineages from both LCS$^+$ treatments harboured ≈ 150 mutations, but some carried ≈ 250 mutations (represented by cross and plus symbols). Surprisingly, lineages from the L-LCS$^-$ treatment (represented by diamond symbols) harboured, for some lineages, more than 350 mutations.

Such large numbers of mutations are indicative of muta-

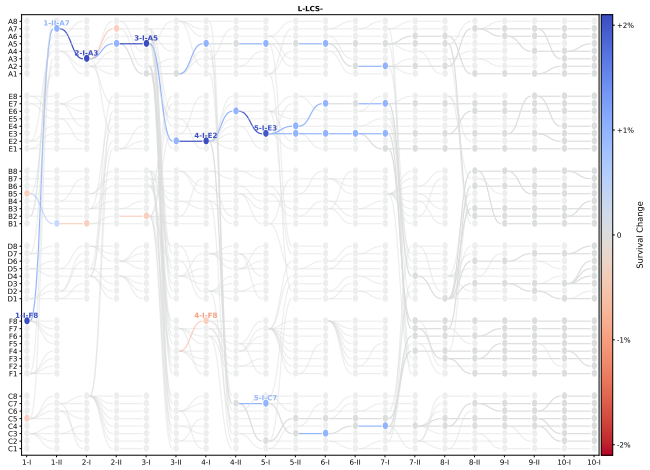

Figure 4. Nodes in the L-LCS⁻ genealogy predicted to mark adaptive change. Lineages are coloured according to predicted change in survival probability relative to the previous cycle. The belief-propagation algorithm used for analysis is described in Supplementary note 1. Here the model is beta with a grid of 100 points. Figure S2 shows this result for all four treatments.

tor genotypes. While known for LCS$^+$ lineages, we nonetheless interrogated all mutational data for evidence of defects in genes known to encode primary components of the methyl-directed mismatch repair (MMR) system (*mutS*, *mutL*, *mutY* and *mutM*). The points in Figure 5, coloured according to genotype, show that microcosms harbouring lineages with large numbers of mutations also carry defects in mis-match repair genes (see Table 1). Again, while known for the *mutS*-based LCS$^+$ lineages, these genotypes acquired additional mutations in MMR genes. For example, eight lineages in Block A of LCS$^+$ evolving in large microcosms acquired a single non-synonymous change in the A/G specific adenine glycosylase *mutY* (G153D). Interestingly this *mutY* mutation did not generate more mutations (Figures 5 and S10), but is associated with a marked bias in the kind of mutations that are found in these lineages (Figure S16).

The greatest number of mutations however were found in LCS$^-$ lineages propagated in large microcosms. As more fully elaborated below, a single *mutL* (L103R) mutation (orange diamond symbols) arose early in the experiment, but seven lineages of block C also acquired an additional *mutS* (G707S) mutation (purple diamond symbols). Figure 6 and Figures S9 to S11 show these mutations in context of the genealogies apparent in each treatment.

As shown in Figure 4, the node marking greatest improvement in survival probability in L-LCS$^-$ is in the vicinity of 2-I-A3 and 2-II-A5. Additional sequencing of these nodes showed that the point of origin of *mutL* (L103R) was immediately prior to 2-II-A5 (See Supplementary note 2-E and Figures S13 to S15 for details of the procedure and iterative use of the algorithm to incorporate new data).

D. Experimental confirmation of adaptive changes.

The combined information provided by the survival probability inference (Section B) and sequencing-information propagation (Section C), points toward an adaptive change having occurred in (or in the vicinity of) microcosm 2-II-A5. In this section, we describe additional experiments conducted to test this hypothesis.

Figure 7a-d shows the results of fitness assays performed around the adaptive points detected by Bayesian inference. These data, composed of measures of the probability to produce viable soma states at the end of Ph I (Figure 7a), probability to transition from soma to germ during Ph I (Figure 7b), probability to switch from germ to soma type during Ph II (Figure 7c), and overall life cycle fitness (Figure 7d), confirm a stepped increase in life cycle fitness of the focal lineage between generation two and four.

Because prior analysis predicted a causal role for the *mutL* (L103R) mutation, this mutation (in genotype 2-II-A5) was reverted, via a single nucleotide change, to the ancestral state. The effects of this change are shown in Figure 7a-d. Data in Figure 7d demonstrate that at the level of overall life cycle performance, the *mutL* (L103R) mutation is the primary cause of enhanced life cycle success. Interestingly the effect is not significant for the two components of Ph I (Figure 7ab), but has a marked impact on ability of the germ stage to switch to the soma state. Further visual evidence for a seminal role of the *mutL* mutation in switching between life cyle states comes from observation of germ cells arising within soma directly on agar plates (Figure S21).

Discussion

The evolution of multicellular life continues to receive attention from both empiricists and theoreticians (Bonner, 2015; Chavhan et al., 2023; Colizzi et al., 2020; Herron et al., 2022; Libby and Rainey, 2013; Michod, 2007; Pichugin et al., 2019; Ratcliff et al., 2013, 2017; Solé and Duran-Nebreda, 2015; Staps et al., 2019). In this work, using the experimental *Pseudomonas* system, we have explored the efficacy of a previously derived genetic switch controlling life cycle transitions, used knowledge of genealogical connections among nascent multicellular entities to predict adaptive events, combined these data with DNA sequence information and, for one particular mutation, demonstrated a causal connection to improved fitness.

The genetic switch, that in a prior experiment had delivered adaptive benefit to competing lineages through significant improvement in control of expression of soma- and germ-like phases, proved, in this work, central to subsequent evolutionary success. This held for continued selection in standard microcosms, but also for selection in large vessels. LCS$^+$ lineages suffered few extinctions during further propagation in standard microcosms, whereas persistence of LCS$^-$ lineages in the same diameter microcosms proved challenging, with frequent death events caused by failures at all three life cycle phases.

Both LCS$^+$ and LCS$^-$ lineages struggled initially to find solutions to producing enduring mats in large diameter microcosms, but in both instances this capacity showed improvement during the course of the experiment. Notable in the L-LCS$^-$ treatment, was the early discovery of a mutation in *mutL* that effectively converted LCS$^-$ to LCS$^+$. In the absence of this mutation – and thus marked improvement in ca-

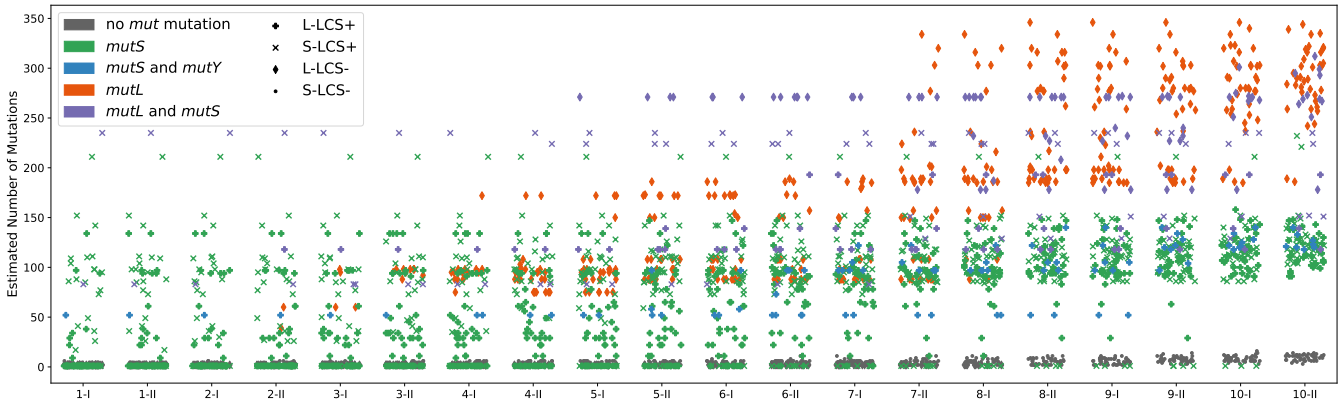

Figure 5. Reconstruction of the number of mutations through time. Each point is the number of new mutations (compared to the ancestor of the genealogy) predicted to be found in a single microcosm at a given phase in each cycle. The inference stems from propagating knowledge of mutations in the final derived genomes of extant lineages backward through the genealogy using the belief-propagation algorithm described in Supplementary note 2. Figure S5 shows the number of identified mutations without reconstruction through the belief-propagation regime. Figure S8 shows the number of mutations associated with each extent lineage (derived directly from genome sequence data).

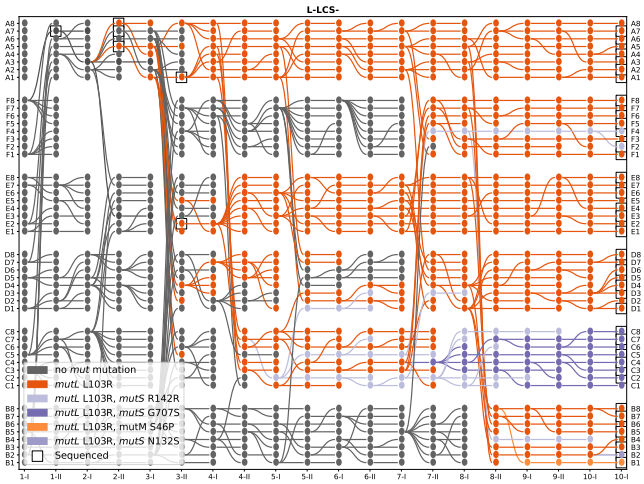

Figure 6. $mutL$ **and** $mutS$ **mutations in the L-LCS⁻ genealogy**. Lineages are colored according to $mutL$ and $mutS$ mutations. The mutation $mutL$ L103R appeared in lineage 2-II-A5 and swept to fixation. Black squares identify sequenced lineages, with the belief-propagation algorithm (described in Supplementary note 2) allowing inferences to be extended to all nodes. Figures S9 to S12 show the same analysis for all four treatments.

pacity to transition between phases of the life cycle – all lineages in the L-LCS⁻ treatment would have gone extinct by the third generation (evident by excluding reproduction events in Figure 3 and following the fate of lineages to the first extinction). Thus, mutator-fuelled switching increased reliability of the transition between life cycle phases, but the elevated mutation rate likely also played a role in discovery of genetic changes that led to the formation of mats not only capable of colonising the surface of large diameter microcosms, but with sufficient structure to ensure persistence over the six days of Ph I.

The prevalence of mutators associated with successful lineages was particularly apparent for lineages evolving in large microcosms and shows that the selective regime strongly favours mutationally-driven genetic switches. These switches deliver benefit through subsequent rounds of selection, despite costs arising from the inevitable load of deleterious mutations.

While L-LCS⁺ lineages were founded by a genotype carrying a *mutS* allele, a further *mutY* G153D mutation arose early in a single Block A lineage and went to fixation by generation 10. That the mutation swept, suggests that it may have contributed to further improvements in the reliability of switching (Figure S2), however, it is not inconceivable that *mutY* G153D hitchhiked along with a mutation that improved performance of the soma phase. Interestingly this mutation did not add to the overall number of mutations (Figures 5 and S10), but it did introduce a marked bias in the kind of mutations found in these lineages (Figure S16). Interrogation of sequence data for changes in repeat-tract length in genes with predicted DGC or PDE activity did not identify obvious candidate effectors of phenotype switching (as previously observed in WspR Hammerschmidt et al. (2014) see Figure 1).

In large microcosms founded by the LCS⁻ lineage, in addition to the early and key *mutL* mutation, a further *mutS* G707S mutation arose in Block C microcosms. As with the *mutY* allele arising in the *mutS* background, the *mutS* G707S mutation, although arising late in the experiment (at generation seven), fixed (in Block C) within a further two generations (Figure S9). While the adaptive significance of this mutation was not further investigated, microcosm 8-I-C4 was identified by `colgen` as a point that marked significant improvement in survival probability (Figure 4).

The fact that no additional mutators evolved in either the S-LCS⁻ or the S-LCS⁺ treatment suggests that additional opportunities for mutator alleles to hitchhike with beneficial mutations were provided in large micrcocosms. This makes intuitive sense given the combination of selective challenge, where founding genotypes were initially poorly adapted, a 40-fold increase in population size (compared to standard microcosms), and the fact that transitions through the life cycle require passage through single cell bottlenecks. Under such conditions there are likely numerous beneficial mutations upon which mutator alleles can hitchhike, moreover, selection is expected to favour cells that switch phenotype early because descendants of such cells have a heightened change

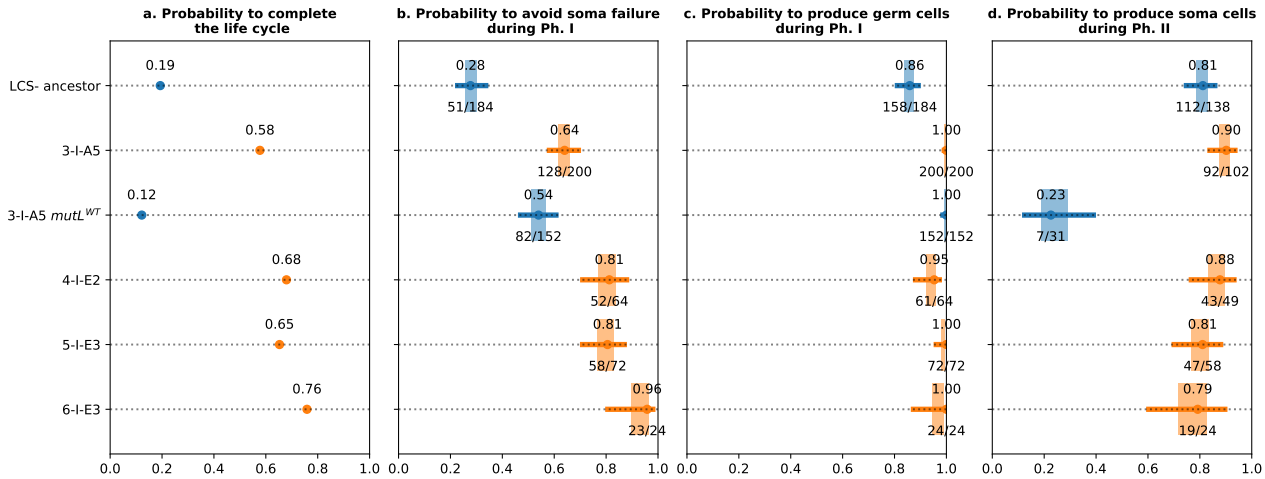

Figure 7. Probability and fitness estimates. Each line corresponds to a genotype taken from selected lineages. Points correspond to the maximum *a posteriori* value for the probability, the fraction of surviving over number of trials is written below the point. The box corresponds to the 50% Bayesian confidence interval and the whiskers correspond to the 95% Bayesian confidence interval (the method is described in Supplementary note 3). Orange depicts genotypes with the *mutL* L103R mutation; blue identifies genotypes without the *mutL* mutation.

of passage through the bottleneck.

A notable difference in this study compared to previous work with the *Pseudomonas* system (Hammerschmidt et al., 2014; Rose et al., 2020) is mode of analysis, particularly that delivered by `colgen`. The first and arguably most valuable component of `colgen` is the simple visual representation of evolutionary dynamics via which evolutionary patterns previously invisible are revealed, allowing, for example, contributions of chance, history and selection to be directly observed. This is further aided by comparisons among the fates of lineages founded by LCS$^+$ and LCS$^-$ genotypes. The former being endowed with the adaptive Muts-WspR based switch – the product of prior evolutionary history – whereas the latter, by virtue of reversion of the *mutS* allele to wild type, has this component of history removed.

LCS$^+$ lineages propagated in standard microcosms suffered few extinction events (Figure 3a), which can be directly attributed to prior evolutionary history and is consistent with adaptive value of the switch. Notable was the worsening of performance after generation three Figure S17. This likely reflects the downside of few initial extinction events, resulting in a shift in the relative contributions of selection acting between- versus within-lineages (Wade, 1978). In the absence of lineage-level death-birth events, selection operates primarily within lineages leading to erosion of traits favouring success of lineages. But as lineage-level death-birth events occur, selection operates both within and between lineages, with, presumably, some equilibrium level ultimately being achieved.

In contrast, for LCS$^-$ lineages propagated in the same standard microcosms, multiple extinction events occurred (Figure 3C). Beyond providing further evidence of the adaptive value of the switch, extinction and concomitant reproduction events are indicative of the hand of chance – both good and bad luck. In fact, as there is no overall improvement in the frequency of extinction events in S-LCS$^-$ lineages – and none detected by `colgen` (Figure S2), it is likely that the observed dynamics are driven almost entirely by chance.

Chance is an inherent factor in all evolutionary change, but a major factor affecting extinction events (Figure 3). Chance underpins ability to transition (by mutation) between life cycle phases, with mutational switches greatly improving the likelihood that transitions are successfully achieved, but chance also plays a role in mat durability with subtle differences determining whether a mat endures the required six-day period. Additionally, chance contributes to whether cells composing the next life cycle phase reach a frequency sufficient to ensure detection.

Extinction, while terminating evolution of affected lineages, provides opportunity for those that are extant to reproduce, and here again, chance is important. Death – often a consequence of bad luck – means that extant lineages, which may be equally susceptible to extinction, serendipitously gain further opportunity to explore genetic (and thus phenotypic) space, and through such exploration, the possibility presents that these lineages, at some future time point, might discover fitness-enhancing mutations: persistence, and its counterpart serendipity, is everything (Palmer and Feldman, 2012).

A single lineage from Block B in the S-LCS$^-$ treatment is a case in point (Figure 3c). The lineage in microcosm b3 produced offspring after the first generation, at generation three, and at generation four, but all failed soon after. Nonetheless, by virtue of persistence at generation five, where the seven competing lineages failed, this lineage went on to leave eight offspring at generation six; by end of the experiment, this single generation-five survivor had given rise to eleven extant offspring. Without further study, the extent to which spread of this lineage reflects adaptive change is unclear, but it is plausible that success to this point was largely a matter of serendipitous chance. This is also reflected in life cycle fitness data in Figure S19 where there is no compelling evidence for the hand of selection, with the fitness of several extant lineages at end of the experiment, being equal or worse than the ancestral type.

A further factor relevant to considerations that recognise the value of sheer persistence, stems from the fact that lineage-level selection, as implemented in the experiments described here, involves a "death-birth" dynamic. This is in contrast to a "birth-death" process in which offspring replace extant collectives, regardless of fitness. While game theory approaches show that death-first dynamics favour the evolution of cooperation (Kaveh et al., 2015; Zukewich et al., 2013), in the context of this experiment a birth-death process would likely diminish the value of persistence.

Also notable in the dynamics of S-LCS$^-$ lineages (but also evident elsewhere) are abrupt extinctions of all lineages (within single blocks) following several generations of successful transitions (Figure 3c). See for example Blocks F and C at Ph I of generation six. While possibly just chance, this more likely reflects deleterious effects of prior mutational history that due to lineages having traversed various mutational paths during prior cycles have exhausted possibilities for realisation of mutations critical for the next life cycle transition.

Turning to LCS$^+$ and LCS$^-$ lineages propagated in large microcosms, similar patterns manifest, however, also apparent are dynamics consistent with the hand of selection. LCS$^+$ lineages, although replete with genetic switch (a product of past history), suffered high levels of extinction during the first few generations, primarily due to premature failure of the soma stage, with such events becoming increasingly rare from generation five. While chance was dominant early on, and the effect of prior history minimal (as expected given that the founding genotypes had not previously experienced selection in large microcosms), sweeps arising from individual lineages, likely underpinned by adaptive change, resulting in fixation of successful types by generation 10.

LCS$^-$ lineages propagated in large microcosms, as described above, narrowly escape wholesale extinction. Having eliminated prior history through elimination of the genetic switch, the fate of these lineages were determined by both the requirement to find solutions to switching and construction of robust mats. Again, as mentioned, a key adaptive change – a mutation in *mutL* – occurred at generation two, with this lineage becoming the progenitor of all extant lineages (across all blocks) at generation 10. A combination of chance and selection were sufficient to overcome – and more than compensate for – prior evolutionary history.

Representation of genealogies via `colgen`, while invaluable in this work is generally application to numerous kinds of lineage selection experiments where mixing of lineages is avoided, as in the "propagule-pool" (as opposed to "migrant-pool" or "mixed") mode of reproduction (Barnett et al., 2024; Rose et al., 2020; Wade and McCauley, 1988). This holds irrespective of whether collectives are clonal Hammerschmidt et al. (2014) or communities Arias-Sánchez et al. (2019); Doulcier et al. (2020); Xie and Shou (2021).

Beyond providing graphic visualisation, `colgen`, by virtue of the underlying Bayesian model, has utility in allowing mutational data obtained from the end of the experiment to be propagated backward throughout the genealogy. This allowed sense to be made of the hundreds of mutations present in mutator lineages, which are typically overwhelmingly difficult to deal with. But in addition, amongst the noise of mutations, `colgen` proved invaluable at identifying microcosms likely to contain adaptive mutations. Detailed investigations into L-LCS$^-$ led to identification of the *mutL* mutation that was pivotal to the success of descendant lineages.

Graphical probabilistic models (such as Bayesian networks) for statistical inference have been used in haplotyping of pedigree (Fishelson et al., 2005), gene network inference (Needham et al., 2007) and genetic diseases risk assessment (Nuel et al., 2017). Bayesian network analysis presents several advantages. Firstly, it is designed to work with partial data: inference can be performed even when sequence data is missing or partial. Secondly, such modes of analyses allow seamless integration of new data, with the possibility of adding new sequencing or fitness information to refine inferences. Thus, Bayesian analysis makes possible iterative protocols that alternate between inferences based on existing data and targeted new experimentation. Finally, the statistical model of observation and transmission of characters is relatively simple to define and can be adjusted for different purposes. While the models used above were minimal in their assumptions, it is possible to conceive and develop more complex mechanistic models as required.

It is evident that life cycles based on mutation can deliver benefits to nascent multicellular types. However, life cycles in extant multicellular organisms are typically effected via developmental mechanisms requiring changes in patterns of gene regulation. While it would be interesting to continue propagation of lineages containing mutation-dependent developmental switches to observe future refinement, it seems unlikely that true developmental control could ever be achieved from such starting points. This has led to a reconsideration of the selective regime imposed here and previously, and particularly reliance on need for soma and germ phases to express distinct colony morphologies on agar plates. Indeed, a redesigned regime that eliminated this requirement, but nonetheless placed significance of formation of soma and germ phases, has shown that lineages capable of transitioning between life cycle phases by developmental control are eminently achievable (Joanna Summers *et al.* forthcoming).

ACKNOWLEDGEMENTS

GD acknowledges the John Templeton Foundation (#62220); GD and PBR acknowledge funding from *Origines et Conditions d'apparition de la vie* (ANR-10-IDEX-001-02). PBR is grateful to the Max Planck Society for generous core support and funding from the Marsden Fund Council from government funding administered by the Royal Society of New Zealand. PBR thanks J. Carlos Hernandez-Beltran and Kaumudi Hassan Prabhakara for comments on a draft of the manuscript. We thank Mathieu Forget for contributions while an intern at the NZIAS.

AUTHOR CONTRIBUTIONS

PBR, experimental design and conception; PR and DR, conduct of experiment; GD development and implementation of `colgen`; all authors analysed data and wrote the MS.

DATA AVAILABILITY

All the data used in this manuscript (genealogy records, reads, alignments, fitness assays) and the code necessary to reproduce all the figures from this dataset is available in the Zenodo repository: https://doi.org/10.5281/zenodo.11170875. `colgen` v2.0b1 used in this manuscript is also available on Zenodo: https://doi.org/10.5281/zenodo.7342768.

Bibliography

Flor I. Arias-Sánchez, Björn Vessman, and Sara Mitri. Artificially selecting microbial communities: If we can breed dogs, why not microbiomes? *PLOS Biology*, 17(8):e3000356, August 2019. doi: 10.1371/journal.pbio.3000356. URL https://journals.plos.org/plosbiology/article?id=10.1371/journal.pbio.3000356.

Michael P. Barnett, Lena Zeller, and Paul B. Rainey. Experimental evolution of evolvability, May 2024. URL https://www.biorxiv.org/content/10.1101/2024.05.01.592015v2.

Andrew J. Black, Pierrick Bourrat, and Paul B. Rainey. Ecological scaffolding and the evolution of individuality. *Nature Ecology & Evolution*, 4(3):426–436, March 2020. doi: 10.1038/s41559-019-1086-9. URL https://www.nature.com/articles/s41559-019-1086-9.

John Tyler Bonner. The origins of multicellularity. *Integrative Biology: Issues, News, and Reviews*, 1(1):27–36, 1998.

John Tyler Bonner. *Life Cycles: Reflections of an Evolutionary Biologist*. Princeton University Press, Princeton, March 2015. ISBN 978-1-4008-7277-0.

Pierrick Bourrat. Evolutionary Transitions in Individuality by Endogenization of Scaffolded Properties. *The British Journal for the Philosophy of Science*, January 2022. doi: 10.1086/719118. URL https://www.journals.uchicago.edu/doi/10.1086/719118.

Leo W. Buss. *The Evolution of Individuality*. Princeton University Press, Princeton, 1987. ISBN 978-0-691-60354-4.

Yashraj Chavhan, Sutirth Dey, and Peter A. Lind. Bacteria evolve macroscopic multicellularity by the genetic assimilation of phenotypically plastic cell clustering. *Nature Communications*, 14(1):3555, June 2023. doi: 10.1038/s41467-023-39320-9. URL https://www.nature.com/articles/s41467-023-39320-9.

Enrico Sandro Colizzi, Renske MA Vroomans, and Roeland MH Merks. Evolution of multicellularity by collective integration of spatial information. *eLife*, 9:e56349, October 2020. doi: 10.7554/eLife.56349. URL https://doi.org/10.7554/eLife.56349.

Daniel E. Deatherage and Jeffrey E. Barrick. Identification of mutations in laboratory evolved microbes from next-generation sequencing data using breseq. *Methods in molecular biology (Clifton, N.J.)*, 1151:165–188, 2014. doi: 10.1007/978-1-4939-0554-6_12. URL https://www.ncbi.nlm.nih.gov/pmc/articles/PMC4239701/.

A. P. Dempster, N. M. Laird, and D. B. Rubin. Maximum Likelihood from Incomplete Data via the EM Algorithm. *Journal of the Royal Statistical Society. Series B (Methodological)*, 39(1):1–38, 1977. URL http://www.jstor.org/stable/2984875.

Guilhem Doulcier. Colgen - Collective Genealogies Visualisation and Analysis, December 2019. URL https://zenodo.org/record/7342768.

Guilhem Doulcier, Amaury Lambert, Silvia De Monte, and Paul B Rainey. Eco-evolutionary dynamics of nested Darwinian populations and the emergence of community-level heredity. *eLife*, 9:e53433, July 2020. doi: 10.7554/eLife.53433. URL https://doi.org/10.7554/eLife.53433.

Guilhem Doulcier, Peter Takacs, Katrin Hammerschmidt, and Pierrick Bourrat. Stability of Ecologically Scaffolded Traits During Evolutionary Transitions in Individuality, August 2023. URL https://www.biorxiv.org/content/10.1101/2023.08.17.553478v1.

Bradley Efron. Bayes' Theorem in the 21st Century. *Science*, 340(6137):1177–1178, June 2013. doi: 10.1126/science.1236536. URL http://science.sciencemag.org/content/340/6137/1177.

Ma'ayan Fishelson, Nickolay Dovgolevsky, and Dan Geiger. Maximum Likelihood Haplotyping for General Pedigrees. *Human Heredity*, 59(1):41–60, 2005. doi: 10.1159/000084736. URL https://www.karger.com/Article/FullText/84736.

Peter Godfrey-Smith. *Darwinian Populations and Natural Selection*. Oxford university Press, Oxford, March 2009. ISBN 978-0-19-160955-8.

J. Griesemer. The Units of Evolutionary Transition. *Selection*, 1(1-3):67–80, January 2001. doi: 10.1556/Select.1.2000.1-3.7. URL https://akademiai.com/doi/abs/10.1556/Select.1.2000.1-3.7.

Richard K. Grosberg and Richard R. Strathmann. The Evolution of Multicellularity: A Minor Major Transition? *Annual Review of Ecology, Evolution, and Systematics*, 38(1):621–654, 2007. doi: 10.1146/annurev.ecolsys.36.102403.114735. URL https://doi.org/10.1146/annurev.ecolsys.36.102403.114735.

Katrin Hammerschmidt, Caroline J. Rose, Benjamin Kerr, and Paul B. Rainey. Life cycles, fitness decoupling and the evolution of multicellularity. *Nature*, 515(7525):75–79, November 2014. doi: 10.1038/nature13884. URL http://www.nature.com/nature/journal/v515/n7525/abs/nature13884.html.

Garrett Hardin. The Tragedy of the Commons. *Science*, 162(3859):1243–1248, December 1968. doi: 10.1126/science.162.3859.1243. URL https://science.sciencemag.org/content/162/3859/1243.

Karl Heilbron, Macarena Toll-Riera, Mila Kojadinovic, and R Craig MacLean. Fitness Is Strongly Influenced by Rare Mutations of Large Effect in a Microbial Mutation Accumulation Experiment. *Genetics*, 197(3):981–990, July 2014. doi: 10.1534/genetics.114.163147. URL https://doi.org/10.1534/genetics.114.163147.

Matthew Herron, Peter L. Conlin, and William Ratcliff. *The Evolution of Multicellularity*. CRC Press, 2022.

Kamran Kaveh, Natalia L. Komarova, and Mohammad Kohandel. The duality of spatial death–birth and birth–death processes and limitations of the isothermal theorem. *Royal Society Open Science*, 2(4):140465, April 2015. doi: 10.1098/rsos.140465. URL https://royalsocietypublishing.org/doi/10.1098/rsos.140465.

Daphne Koller and Nir Friedman. *Probabilistic graphical models: principles and techniques*. MIT press, 2009.

Anna Koza, Olena Moshynets, Wilfred Otten, and Andrew J Spiers. Environmental modification and niche construction: developing O2 gradients drive the evolution of the Wrinkly Spreader. *The ISME Journal*, 5(4):665–673, April 2011. doi: 10.1038/ismej.2010.156. URL https://doi.org/10.1038/ismej.2010.156.

Eric Libby and Paul B. Rainey. Eco-Evolutionary Feedback and the Tuning of Proto-Developmental Life Cycles. *PLOS ONE*, 8(12):e82274, December 2013. doi: 10.1371/journal.pone.0082274. URL http://journals.plos.org/plosone/article?id=10.1371/journal.pone.0082274.

John Maynard Smith and Eors Szathmary. *The Major Transitions in Evolution*. W.H. Freeman, Oxford, 1995. ISBN 0-7167-4525-9.

Richard E. Michod. *Darwinian Dynamics: Evolutionary Transitions in Fitness and Individuality*. Princeton University Press, Princeton, January 2000. ISBN 978-0-691-05011-9.

Richard E. Michod. Evolution of individuality during the transition from unicellular to multicellular life. *Proceedings of the National Academy of Sciences*, 104(suppl 1):8613–8618, May 2007. doi: 10.1073/pnas.0701489104. URL https://www.pnas.org/content/104/suppl_1/8613.

Chris J. Needham, James R. Bradford, Andrew J. Bulpitt, and David R. Westhead. A Primer on Learning in Bayesian Networks for Computational Biology. *PLOS Computational Biology*, 3(8):e129, August 2007. doi: 10.1371/journal.pcbi.0030129. URL http://journals.plos.org/ploscompbiol/article?id=10.1371/journal.pcbi.0030129.

Gregory Nuel, Alexandra Lefebvre, and Olivier Bouaziz. Computing Individual Risks Based on Family History in Genetic Disease in the Presence of Competing Risks. *Computational and Mathematical Methods in Medicine*, 2017. URL https://www.hindawi.com/journals/cmmm/2017/9193630/abs/.

Samir Okasha. *Evolution and the levels of selection*, volume 16. Clarendon Press, Oxford, 2006.

Michael E. Palmer and Marcus W. Feldman. Survivability Is More Fundamental Than Evolvability. *PLOS ONE*, 7(6):e38025, June 2012. doi: 10.1371/journal.pone.0038025. URL https://journals.plos.org/plosone/article?id=10.1371/journal.pone.0038025.

Yuriy Pichugin, Hye Jin Park, and Arne Traulsen. Evolution of simple multicellular life cycles in dynamic environments. *Journal of The Royal Society Interface*, 16(154):20190054, May 2019. doi: 10.1098/rsif.2019.0054. URL https://royalsocietypublishing.org/doi/full/10.1098/rsif.2019.0054.

Paul B. Rainey and Silvia De Monte. Resolving Conflicts During the Evolutionary Transition to Multicellular Life. *Annual Review of Ecology, Evolution, and Systematics*, 45(1):599–620, 2014. doi: 10.1146/annurev-ecolsys-120213-091740. URL http://dx.doi.org/10.1146/annurev-ecolsys-120213-091740.

Paul B. Rainey and Benjamin Kerr. Cheats as first propagules: A new hypothesis for the evolution of individuality during the transition from single cells to multicellularity. *BioEssays*, 32(10):872–880, October 2010. doi: 10.1002/bies.201000039. URL http://onlinelibrary.wiley.com/doi/10.1002/bies.201000039/abstract.

Paul B. Rainey and Katrina Rainey. Evolution of cooperation and conflict in experimental bacterial populations. *Nature*, 425(6953):72–74, September 2003. doi: 10.1038/nature01906. URL https://www.nature.com/articles/nature01906.

Paul B Rainey, Philippe Remigi, Andrew D Farr, and Peter A Lind. Darwin was right: where now for experimental evolution? *Current Opinion in Genetics & Development*, 47:102–109, December 2017. doi: 10.1016/j.gde.2017.09.003. URL http://www.sciencedirect.com/science/article/pii/S0959437X17300801.

William C. Ratcliff, Matthew D. Herron, Kathryn Howell, Jennifer T. Pentz, Frank Rosenzweig, and Michael Travisano. Experimental evolution of an alternating uni- and multicellular life cycle in Chlamydomonas reinhardtii. *Nature Communications*, 4(1):2742, November 2013. doi: 10.1038/ncomms3742. URL https://www.nature.com/articles/ncomms3742.

William C. Ratcliff, Matthew Herron, Peter L. Conlin, and Eric Libby. Nascent life cycles and the emergence of higher-level individuality. *Phil. Trans. R. Soc. B*, 372(1735):20160420, December 2017. doi: 10.1098/rstb.2016.0420. URL http://rstb.royalsocietypublishing.org/content/372/1735/20160420.

Caroline J. Rose, Katrin Hammerschmidt, Yuriy Pichugin, and Paul B. Rainey. Meta-population structure and the evolutionary transition to multicellularity. *Ecology Letters*, 23(9):1380–1390, 2020. doi: 10.1111/ele.13570. URL https://onlinelibrary.wiley.com/doi/abs/10.1111/ele.13570.

Ricard V. Solé and Salva Duran-Nebreda. In Silico Transitions to Multicellularity. In Iñaki Ruiz-Trillo and Aurora M. Nedelcu, editors, *Evolutionary Transitions to Multicellular Life: Principles and mechanisms*, pages 245–266. Springer Netherlands, Dordrecht, 2015. ISBN 978-94-017-9642-2. doi: 10.1007/978-94-017-9642-2_13. URL https://doi.org/10.1007/978-94-017-9642-2_13.

Merlijn Staps, Jordi van Gestel, and Corina E. Tarnita. Emergence of diverse life cycles and life histories at the origin of multicellularity. *Nature Ecology & Evolution*, 3(8):1197–1205, August 2019. doi: 10.1038/s41559-019-0940-0. URL https://www.nature.com/articles/s41559-019-0940-0.

Michael J. Wade. A Critical Review of the Models of Group Selection. *The Quarterly Review of Biology*, 53(2):101–114, 1978. URL http://www.jstor.org/stable/2826195.

Michael J. Wade and David E. McCauley. Extinction and Recolonization: Their Effects on the Genetic Differentiation of Local Populations. *Evolution*, 42(5):995–1005, 1988. doi: 10.2307/2408915. URL http://www.jstor.org/stable/2408915.

Li Xie and Wenying Shou. Steering ecological-evolutionary dynamics to improve artificial selection of microbial communities. *Nature Communications*, 12(1):6799, November 2021. doi: 10.1038/s41467-021-26647-4. URL https://www.nature.com/articles/s41467-021-26647-4.

Joshua Zukewich, Venu Kurella, Michael Doebeli, and Christoph Hauert. Consolidating Birth-Death and Death-Birth Processes in Structured Populations. *PLOS ONE*, 8(1):e54639, January 2013. doi: 10.1371/journal.pone.0054639. URL https://journals.plos.org/plosone/article?id=10.1371/journal.pone.0054639.

Supplementary Information

Content:

- Figure S1 page 12
- Figure S2 page 13
- Supplementary note 1 page 14
- Supplementary note 2 page 17
- Supplementary note 3 page 24
- Figure S21 page 26

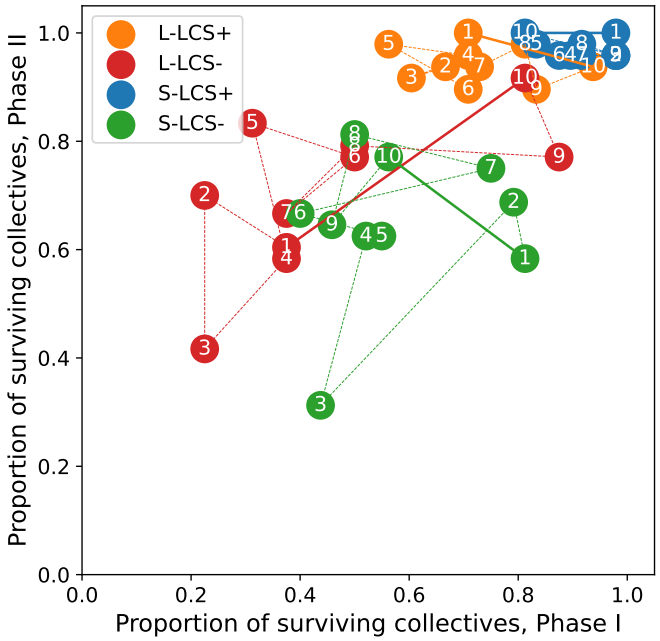

Figure S1. Proportion of surviving lineages in Ph I and Ph II for each cycle. Each circle corresponds to the proportion of surviving lineages for the cycle that is labelled. Each color is a different treatment, LCS$^+$: Lineage 17 from Hammerschmidt et al. (2014) with a life cycle switch, LCS$^-$: same lineage with switching capacity eliminated, S: standard microcosms, L: large microcosms. The dashed lines link consecutive cycles, the thick lines link the first and last cycle, representing the resulting change over the whole experiment. Note that for all treatment but L-LCS$^-$, there exists a trade-off between survival in the two phases.

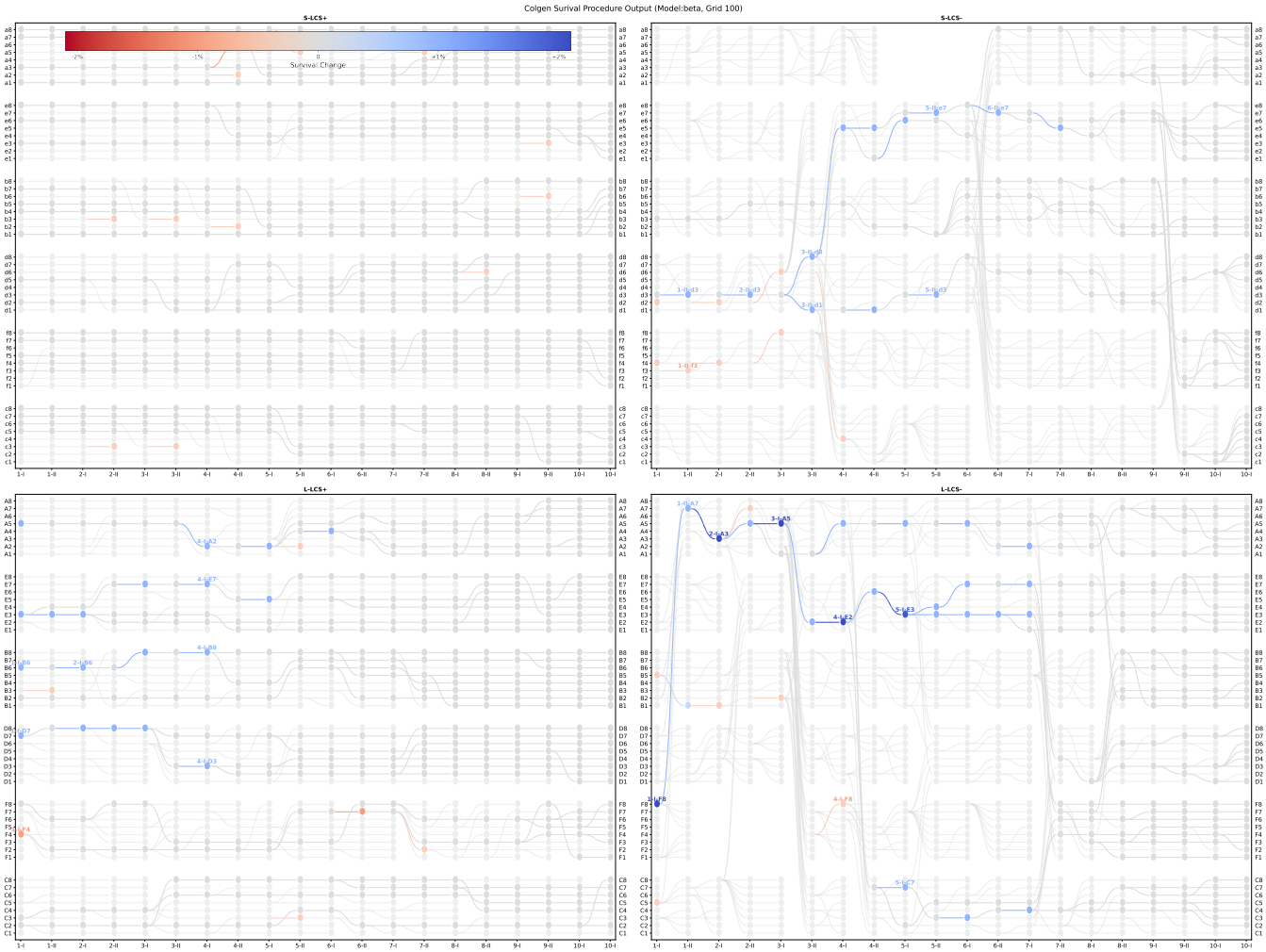

Figure S2. Nodes in lineages at which the probability of survival improves. Model Beta, Grid:100, Sigma-max:1500,

Supplementary Note 1: Adaptive value estimation

We describe a method to assign to each collective within the genealogy a most probable adaptive value. In technical terms, the "most probable adaptive value" refers to a maximum likelihood estimation (MLE) that is a way to assign, under a defined graphical probabilistic model, a value to a parameter that maximise the probability of the observed result. The adaptive value is here a hidden variable: one does not simply observe the adaptive value of a collective, but performs experiments that provide information on its true value.

This endeavour requires first encoding of both the observations and the hidden characteristics of the collectives in a model, that takes the form of a joint probability distribution. Second, a method to find the most likely assignation of an adaptive value to each culture within the genealogy, for a given mutation rate, will be presented. Conversely, parameter inference allows assignment of the most likely value of a mutation rate for a given configuration. Finally, the iterative method of Expectation-Maximisation will be used to concurrently fit to the data both the adaptive value and the mutation rate.

A. Model structure.

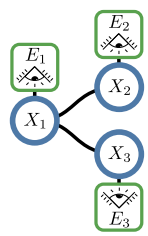

Figure S3. Bayesian Network. Bayesian network corresponding to a genealogy of three collectives. Collective 1 has two offsprings: collectives 2 and 3. Vertices are random variables, edges are conditional dependence. The hidden variables X encode the survival probability of the collectives, while the observed variables E encode the outcome of the experiment (survived or not).

Each collective genealogy $\mathcal{T} = (V, \mathcal{E})$ is a forest containing N numbered vertices: $V = 1...N$ which are the collectives, and an edge linking each collective i to its parent p_i : $\mathcal{E} = (i, p_i)_{i=1...N}$.

The model assigns to each collective an observed and a hidden variable. For a collective i, let E_i be the random variable encoding whether this collective went extinct ($E_i = 1$) or not ($E_i = 0$). In the field of probabilistic graphical models the observed values such as the $(E_i)_{i=1...N}$ are called "evidence".

The first assumption of the model is that there exists a hidden random variable for each collective i, called X_i, representing its survival probability. In probabilistic terms, this means that the conditional probability of extinction of a collective i knowing the value of the survival probability x_i is exactly the value of x_i:

$$\mathbb{P}(E_i = e_i | X_i = x_i) = \begin{cases} x_i & \text{if } e_i = 0 \\ 1 - x_i & \text{if } e_i = 1 \end{cases} \tag{1}$$

The second assumption of the model is that the survival probability of a collective is transmitted from one collective generation to the next, with an unbiased small variation. In probabilistic terms it means that if the parent collective has survival probability x_{p_i}, then the survival probability of its offspring collective follows a distribution with mean x_{p_i} Several probability distributions families can be used. Colgen implement two of them: a beta distribution and a "jump" distribution family parameterized by a single scalar σ.

For the beta distribution:

$$\mathbb{P}(X_i \in A | X_{p_i} = x_{p_i}) = C \int_A \frac{x^{\sigma x_{p_i}} (1-x)^{\sigma(1-x_{p_i})}}{B(1+\sigma x_{p_i}, 1+\sigma(1-x_{p_i}))} \tag{2}$$

with $A \subset [0,1]$, $B(u,v) = \frac{\Gamma(u)\Gamma(v)}{\Gamma(u+v)}$, Γ the Gamma function, and C a scaling factor ensuring that $\int_0^1 \mathbb{P}(X_i = x | X_{p_i} = x_{p_i}) dx = 1$.

For the jump distribution:

$$\mathbb{P}(X_i = p_i | X_{p_i} = x_{p_i}) = \begin{cases} \sigma + (1-\sigma)C & \text{if } X_i = x_{p_i} \\ (1-\sigma)C & \text{otherwise.} \end{cases} \tag{3}$$

With x_i, x_{p_i} both in $(1/C, 2/C...k/C, 1)$, and C a scaling factor ensuring that $\int_0^1 \mathbb{P}(X_i = x | X_{p_i} = x_{p_i}) dx = 1$.

During the experiment, the values of $E_i = e_i$ (extinct or not) are observed, whereas the values of X_i are "hidden".

B. Bayesian inference.

Consider a collective i with associated survival probability X_i and experimental outcome E_i. The prior probability distribution of X_i is given by Equation 2. Consider for an instant that x_{p_i}, the adaptive value of its parent is a fixed parameter. Bayes' Theorem gives the expression of the probability of X_i, conditional on the observed value of E_i:

$$\mathbb{P}(X_i|E_i) = \frac{\mathbb{P}(E_i|X_i)\mathbb{P}(X_i)}{\mathbb{P}(E_i)} \tag{4}$$

Where $\mathbb{P}(X_i)$ is the prior probability of X_i, $\mathbb{P}(E_i|X_i)$ is the observation model from Equation 1 and $\mathbb{P}(E_i)$ is the probability of the evidence. The maximum likelihood estimate (or more precisely the maximum a posteriori estimate, MAP) of the value of X_i is given by taking the value of x that maximises $\mathbb{P}(X_i = x|E_i)$, note that the value of the MAP does not depend on $\mathbb{P}(E_i)$, which is a simple scaling constant. Observing the outcome of the experiment (survival or extinction) has an effect on the posterior: the whole distribution (and consequently the MAP) is shifted toward higher values if the collective survived, or lower values if the collective went extinct.

The problem lies, as often in Bayesian statistics, in the prior probability of X_i (Efron, 2013). Indeed, in the context of the experiment, this probability depends on the state of all the ancestors of the collective i. Applying Bayes theorem to all those interdependent observations quickly becomes a complex undertaking without a proper method. Evidence propagation, presented hereafter, is this optimal method.

The next section details the technical steps required to find the most probable values of X_i throughout the genealogy.

C. Finding the most likely configuration of the genealogy.

The configuration of the full genealogy is the knowledge of the state of all vertices. Hence, it is encoded as a joint distribution that maps each configuration to a probability:

$$(\mathbf{x}, \mathbf{e}) \mapsto \mathbb{P}(\mathbf{X} = \mathbf{x}, \mathbf{E} = \mathbf{e}) \tag{5}$$

Where bold letters are used to represent vectors of dimension N, $\mathbf{x} = (x_i)_{i\in V}$, $\mathbf{X} = (X_i)_{i\in V}$, $\mathbf{E} = (E_i)_{i\in V}$, $\mathbf{e} = (e_i)_{i\in V}$.

The likelihood of a given set of adaptive values $\mathbf{x}$ is defined as the probability of observing this value, conditional on the state of all collectives:

$$L(\mathbf{x}) = \mathbb{P}(\mathbf{X} = \mathbf{x}|\mathbf{E} = \mathbf{e}) \tag{6}$$

The maximum a posteriori configuration of the network is given by finding the value of $\mathbf{x}$ that maximises $L(\mathbf{x})$. The naïve, brute force method to find this value is to compute the L for all $\text{Card}(\omega)^N$ possible configurations (where $\text{Card}(\omega)$ is the number of possible value of X. If the adaptive value is discretised in a hundred of values, this gives 100^{48} computations (in the order of the number of atom of earth $\approx 10^{50}$, and way too much even for modern computers).

However, the probability distribution can be efficiently factorised thanks to the definition of conditional probabilities whose structure is represented in the graph: each pair of nodes not linked by an edge is conditionally independent of one another. As an example consider the small network in Figure S3. The factorisation will go like this:

$$\begin{aligned}
\mathbf{x}^* &= \arg\max_{\mathbf{X}} \mathbb{P}(X_1, X_2, X_3|E_1, E_2, E_3) \\
&= \arg\max_{\mathbf{X}} \frac{\mathbb{P}(X_1, X_2, X_3, E_1, E_2, E_3)}{\mathbb{P}(E_1, E_2, E_3)} \quad \text{(Definition of conditional probability)} \\
&= \arg\max_{\mathbf{X}} \mathbb{P}(X_1, X_2, X_3, E_1, E_2, E_3) \quad \text{(Denominator constant with respect to}\mathbf{x}\text{)} \\
&= \arg\max_{\mathbf{X}} \mathbb{P}(X_1)\mathbb{P}(E_1|X_1)\mathbb{P}(X_2|X_1)\mathbb{P}(E_2|X_2)\mathbb{P}(X_3|X_1)\mathbb{P}(E_3|X_3) \quad \text{(Conditional independence)} \\
&= \arg\max_{X_1} \left[\underbrace{\mathbb{P}(X_1)\mathbb{P}(E_1|X_1)}_{\phi_1(X_1)} \underbrace{\arg\max_{X_2} (\mathbb{P}(X_2|X_1)\mathbb{P}(E_2|X_2))}_{\phi_2(X_1)} \underbrace{\arg\max_{X_3} (\mathbb{P}(X_3|X_1)\mathbb{P}(E_3|X_3))}_{\phi_3(X_1)} \right] \\
&= \arg\max_{X_1} \phi_1(X_1)\phi_2(X_1)\phi_3(X_1) \quad \text{(Variable elimination of } X_1, X_2\text{)}
\end{aligned}$$

Additionally, the "maximum" operation is distributive, which allows for efficient computation of local maxima (ϕ_2, ϕ_3, called messages) that depend on a single variable. This constitutes the essence of the Max-Product Belief propagation algorithm (Koller and Friedman (2009), Chapter 13).

D. Expectation-Maximisation procedure.

Now, how can one find the value of the parameters of the model ? The Expectation-Maximisation (EM) algorithm (Dempster et al., 1977), which might be one of the most influential advances in modern computational statistics and is widely used in Gaussian Mixtures, and Hidden Markov Models, provides an iterative solution.

First, note that for any given configuration of the network (values of $\mathbf{X}$ and $\mathbf{E}$), finding the maximum likelihood estimate of the parameter (mutation rate σ) is a simple matter of computing the value of the parameter that maximises the likelihood $\mathbb{P}(\mathbf{X}, \mathbf{E})$).

Now, starting from an arbitrary value of parameters (say, $\sigma = \frac{1}{2}$), one may compute the Maximum A Posteriori configuration of the network, that assigns a value to each hidden variable. This constitutes the Expectation (E) step. Then, a new value of the parameter is computed using the Maximum of Likelihood estimate. This constitutes the maximisation step (M). The procedure can be iterated until convergence. This algorithm is guaranteed to reach a local maximum in likelihood, but may not reach the global maximum. However, its conceptual simplicity means that it is often the best heuristic available for practical applications.

E. Pre-processing specific to the present life-cycle experiment.

The mat-selection experiment described in the main text features two alternating phases (selection for germ, selection for soma) involving very different processes and are likely to yield different survival probabilities. As a consequence, two sub-trees were extracted for each genealogy, one for Ph I and the other for Ph II (Figure S4) and analysed separately.

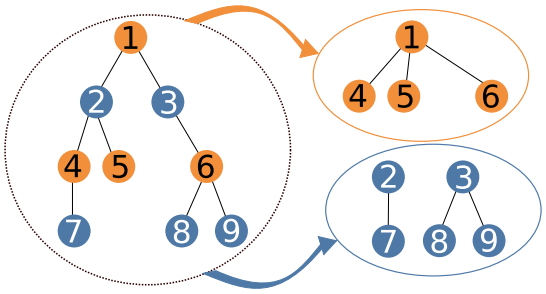

Figure S4. Subtree extraction procedure. Phase 1 (selection for a somatic mat and germ-like cells) and phase 2 (selection for the reversion to soma-like cells) are qualitatively different and are treated separately. In order to achieve this, each collective genealogy is split into a phase 1 and a phase 2 tree that are analysed on their own, and re-assembled for visualisation.

References.

Dempster, A. P., Laird, N. M., and Rubin, D. B. (1977). Maximum Likelihood from Incomplete Data via the EM Algorithm. *Journal of the Royal Statistical Society. Series B (Methodological)*, 39(1):1–38.

Efron, B. (2013). Bayes' Theorem in the 21st Century. *Science*, 340(6137):1177–1178.

Hammerschmidt, K., Rose, C. J., Kerr, B., and Rainey, P. B. (2014). Life cycles, fitness decoupling and the evolution of multicellularity. *Nature*, 515(7525):75–79.

Koller, D. and Friedman, N. (2009). *Probabilistic graphical models: principles and techniques.* MIT press.

Supplementary Note 2: Sequencing and mutation history reconstruction

A. Number of mutation identified by direct sequencing.

Figure S5 represents the number of mutations identified in each sequenced lineage. Note that the L-LCS⁻ has a significantly higher number of mutations than S-LCS⁻ at cycle 10 depsite being started with the same genotype. It seems that it has became a hypermutator line.

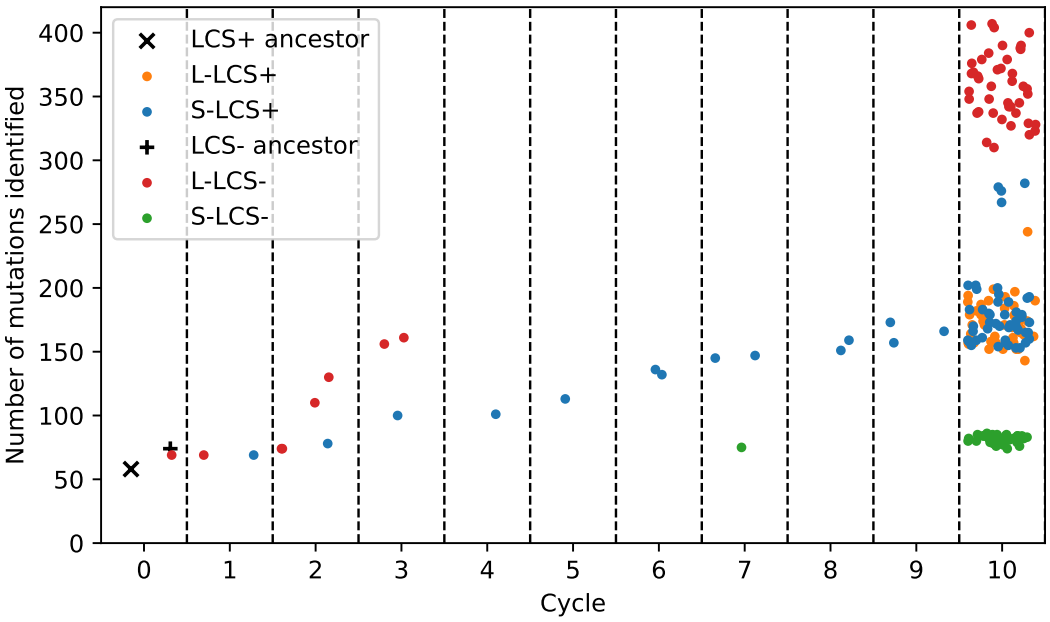

Figure S5. Number of mutations identified by direct sequencing. Each circle is a sequenced culture. Mutations are identified by mapping shorts read onto the reference SBW25 genome (GCF000009225_2). See materials and methods for details. The x-axis correspond to the cycle, the x-position is randomized within each cycle to avoid overlap. Compare this figure with Figure 5 (Note that in Figure 5, the mutations present in the ancestor are filtered out) and Figure S6 that show this data propagated through the whole genealogy.

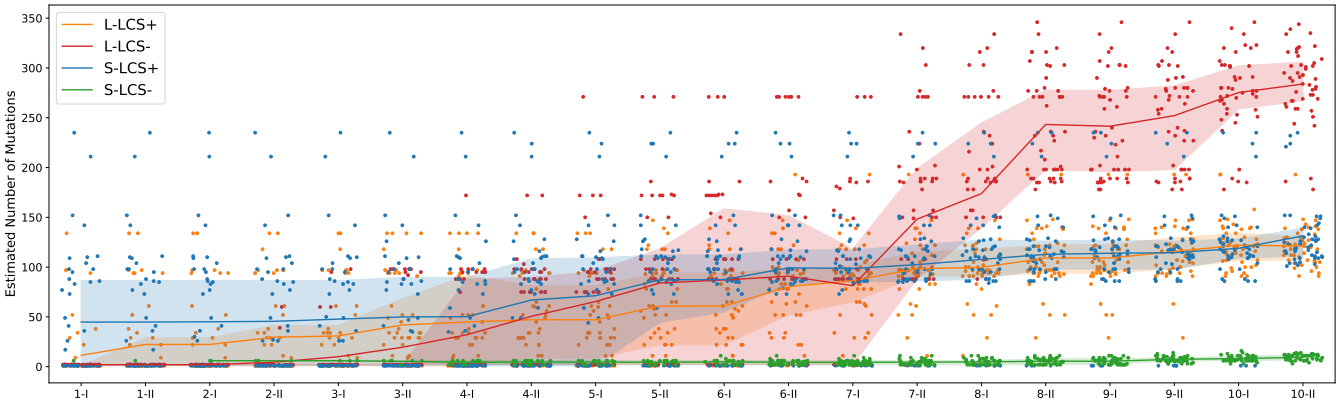

Figure S6. Number of new mutations reconstructed by belief propagation. Each circle is a sequenced genotype. The x-axis corresponds to generation of the life cycle, the x-position is randomized within each cycle to avoid overlap. Compare this figure with Figure S5 that shows these data only for mutations identified by sequencing (and includes mutations present in the ancestor). Lines correspond to the average number of mutations per treatment, shaded areas correspond to 50%-quantils.

B. Propagation of mutational data from sequencing through genealogies.

We use the belief propagation algorithm presented in Supplementary note 1, but the hidden variable X_i is now the presence ($X_i = 1$) or absence ($X_i = 0$) of the mutation within the lineage. The observed variable E_i is replaced by a conditionally Bernoulli variable O_i encoding the event "the mutation of interest was identified in sequences obtained from collective i" for the genotype that was sequenced. The observation model must be specified:

$$\mathbb{P}(0_i = i | X_i = j) = \begin{bmatrix} p & 1-p \\ 1-q & q \end{bmatrix}_{i,j} \tag{7}$$

Where p and q represent, respectively, the probability of true negative and true positive reporting. In the following $p = q = 1$. Finally, the heredity model is specified as:

$$\mathbb{P}(X_i = i | X_{p_i} = j) = \begin{bmatrix} 1-\mu & \mu \\ \mu_r & 1-\mu_r \end{bmatrix}_{i,j} \tag{8}$$

Where μ is the probability that the mutation appears within one cycle and μ_r the probability of losing the mutation. In the main text, arbitrary values of $\mu = 0.001$ and $\mu_r = 0.00001$ have been selected.

C. Number of mutations.

Figures S6 and S8 represent the number of mutations predicted in each node by the belief propagation algorithm.

D. Mut mutations.

We focused on the mutations in genes known to encode components of the methyl-directed mismatch repair system (*mut* family: *mutS*, *mutL*, *mutY* and *mutM*, 17 mutations were identified, see Table 1). The results are shown on the genealogies in Figures S9 to S12.

Table 1. Description of the mutations in the methyl-directed mismatch repair system identified in the dataset. Figure S7 shows in which lineages they were identified.

Gene	Position	Mutation	Annotation	Description
mutY ←	355688	C→T	G153D (GGC→GAC)	A/G-specific adenine glycosylase
mutL →	586966	C→T	S5L (TCG→TTG)	DNA mismatch repair protein
mutL →	587050	A→G	E33G (GAG→GGG)	DNA mismatch repair protein
mutL →	587260	T→G	L103R (CTG→CGG)	DNA mismatch repair protein
mutL →	587555	C→T	L201L (CTC→CTT)	DNA mismatch repair protein
mutL →	587737	A→G	N262S (AAC→AGC)	DNA mismatch repair protein
mutL →	588126	(G)5→6	coding (1174/1902 nt)	DNA mismatch repair protein
mutL →	588551	C→T	A533A (GCC→GCT)	DNA mismatch repair protein
mutS ←	1300356	C→T	G707S (GGC→AGC)	DNA mismatch repair protein
mutS ←	1300673	+A	coding (1802/2592 nt)	DNA mismatch repair protein
mutS ←	1300783	A→G	R564R (CGT→CGC)	DNA mismatch repair protein
mutS ←	1300986	T→G	T497P (ACC→CCC)	DNA mismatch repair protein
mutS ←	1301392	A→G	R361R (CGT→CGC)	DNA mismatch repair protein
mutS ←	1302049	A→G	R142R (CGT→CGC)	DNA mismatch repair protein
mutS ←	1302080	T→C	N132S (AAC→AGC)	DNA mismatch repair protein
mutS ← / ← PFLU_1165	1302576	G→A	intergenic (-102/+68)	DNA mismatch repair protein/putative membrane protein
mutM ←	6343361	A→G	S46P (TCC→CCC)	formamidopyrimidine-DNA glycosylase

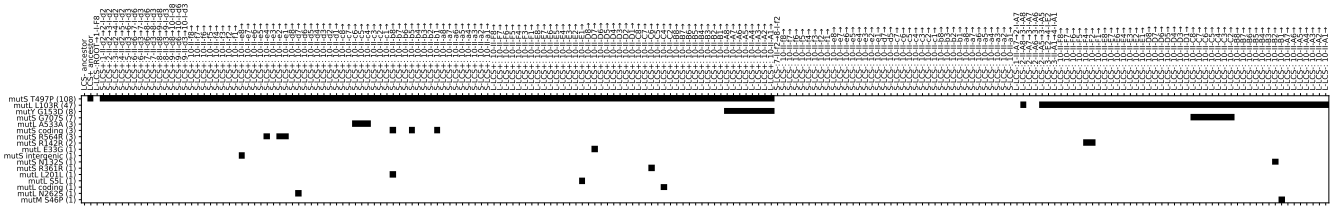

Figure S7. Identified mutations of the methyl-directed mismatch repair system in the sequenced genomes. A black square indicate that the mutation was identified. See Table 1 for a description of the mutations.

E. Finding the location of the L103R *mutL* mutation.

Figures S13 to S15 explain how we pinpoint the location of L103R *mutL*.

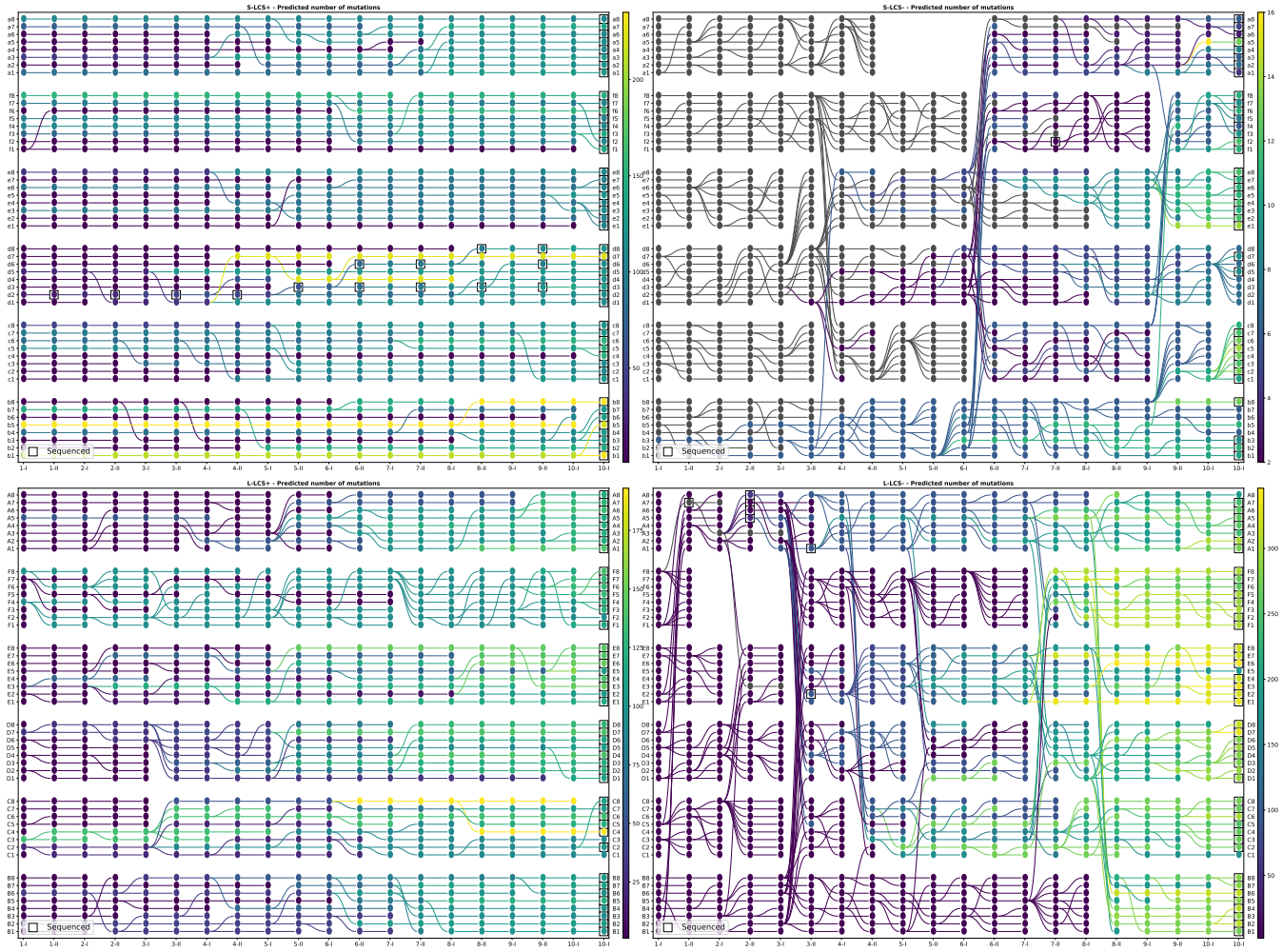

Figure S8. Estimated number of mutations per node. Sequenced genotypes are marked with a black square.

When we only had the endpoints of L-LCS$^-$ sequenced, the L103R *mutL* mutation was in all the sequenced nodes, so the best prediction that could be done was "in the last common ancestor" See Figure S13.

However, the information obtained through the survival estimation algorithm prompted further investigation around 2-II-A5 and 3-II-E2, so additional sequencing was conducted of nodes 1-II-A7, 2-II-A5, 2-II-A6, 2-II-A7, 2-II-A8, 3-II-E2 and 3-II-A1. The mutation is present in 2-II-A5, 2-II-A8, 3-II-E2 and 3-II-A1 and absent in the other nodes (Figure S14).

The propagation procedure of `colgen` output two origins of mutL (Figure S15), in 2-II-A5 and 2-II-A8, because it is highly unlikely that it was in 1-I-A3 and was not transmitted to 2-II-A6 and 2-II-A7.

This mean that the mutation probably appeared between the single cell bottleneck at the end of 1-II-A7 and the single cell bottleneck at 2-II-A5 and 2-II-A8. However, not all cells within 1-I-A3 carry the mutation.

F. Mutation bias in *mutY*.

Figure S16 shows the mutation biais in lineages with a *mutY* mutation.

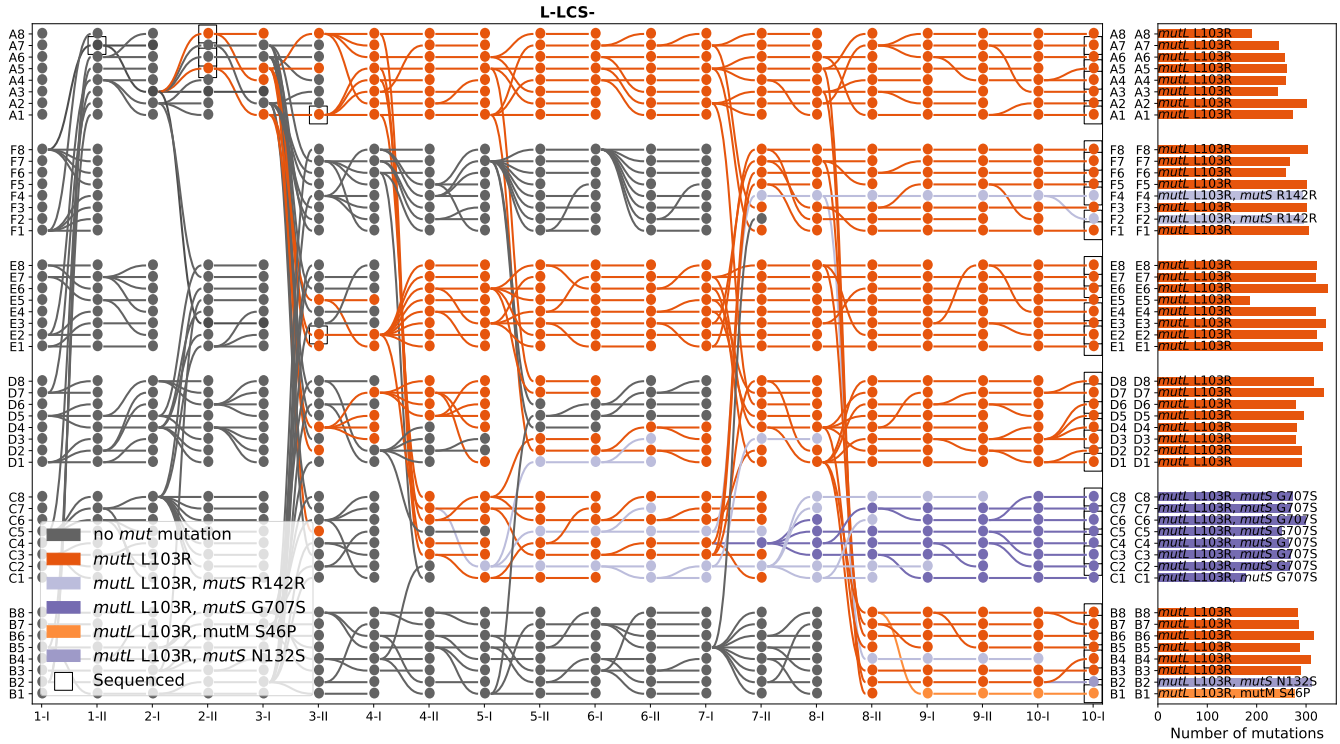

Figure S9. Mut mutations and number of mutations at the endpoint for L-LCS^{-}

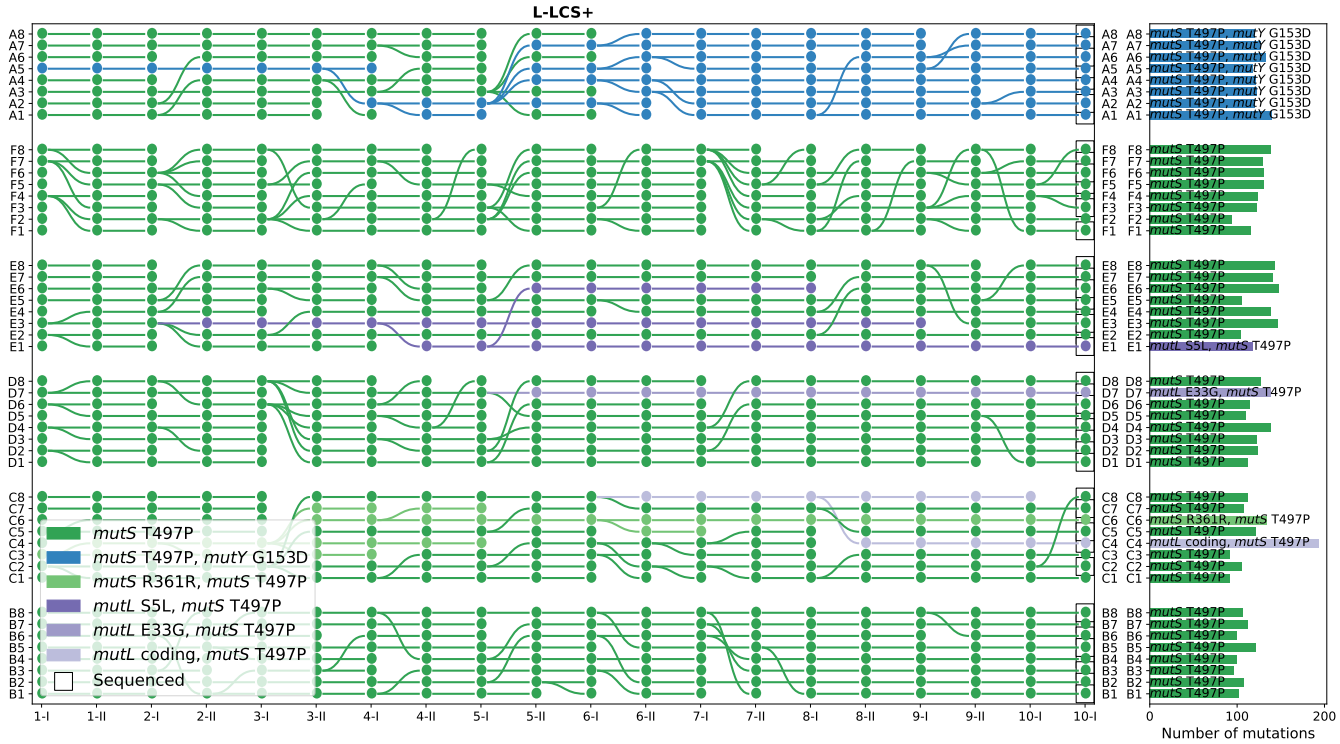

Figure S10. Mut mutations and number of mutations at the endpoint for L-LCS^{+}

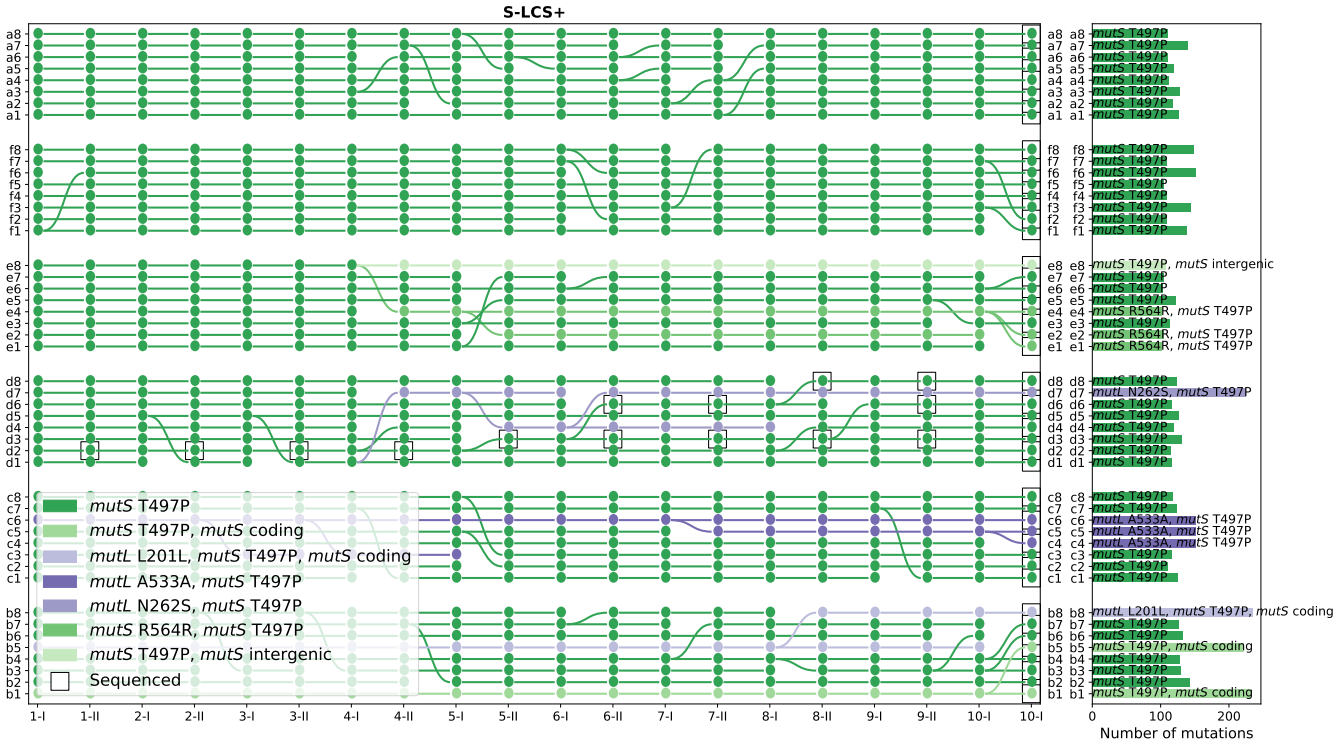

Figure S11. Mut mutations and number of mutations at the endpoint for S-LCS^{+}

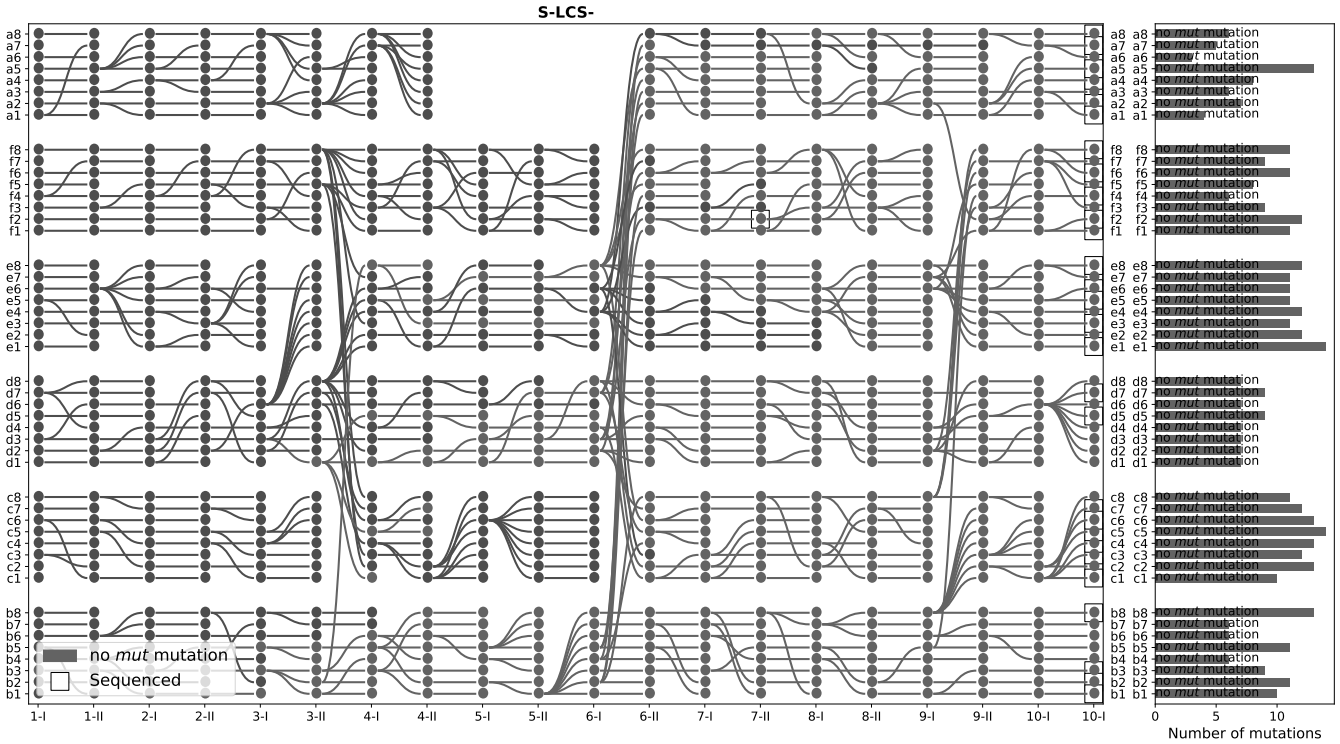

Figure S12. Mut mutations and number of mutations at the endpoint for S-LCS^{-}

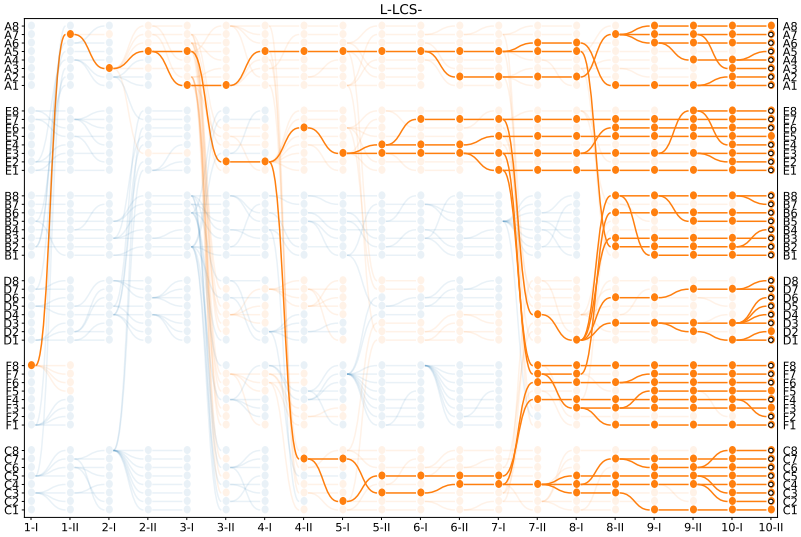

Figure S13. MutL origin, when only using the data from the endpoint.

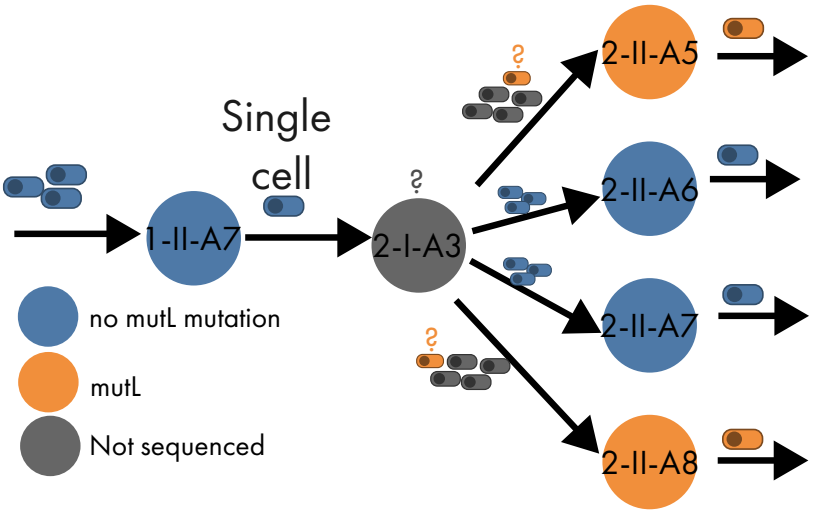

Figure S14. Sequencing result around 2-II-A5

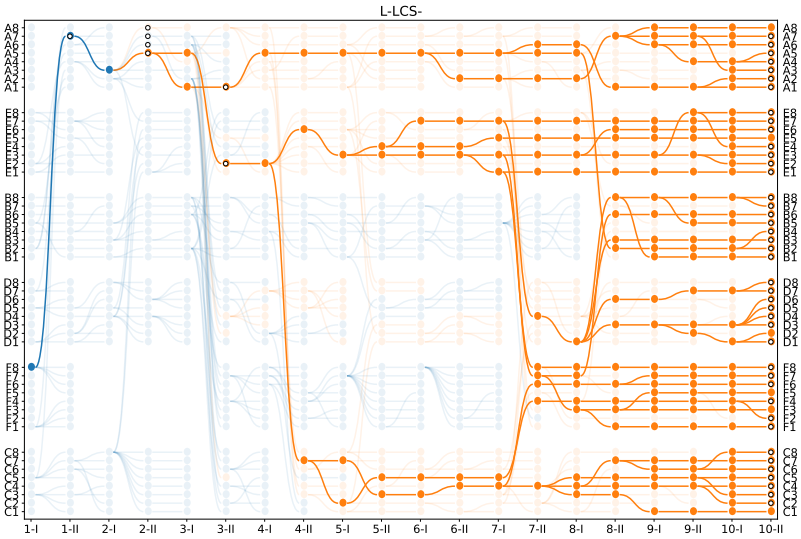

Figure S15. MutL origin, when using all the sequencing data.

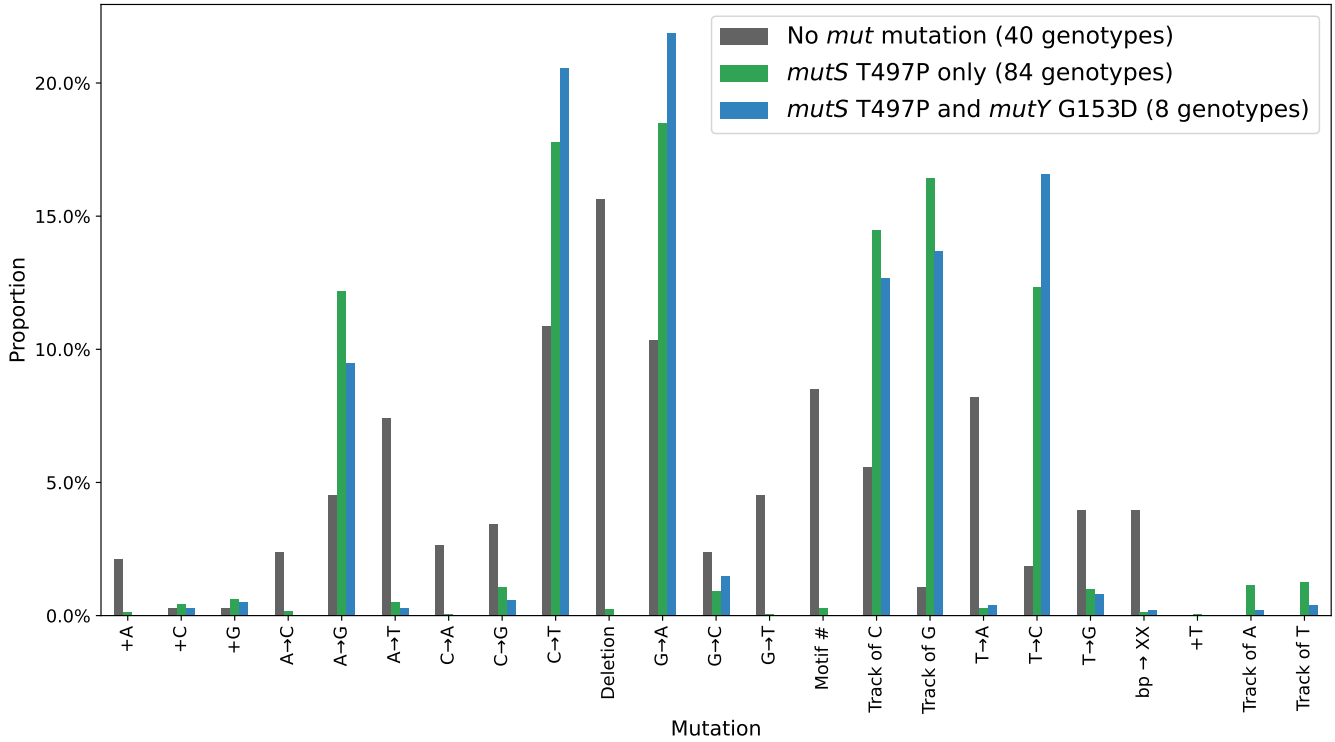

Figure S16. Kind of mutations in microcosms with no mut mutation, with only *mutS* T497P and with both *mutS* T497P and *mutY* G153D mutations.

Supplementary Note 3: Fitness assays

Previously, measures of fitness have involved lineage-level competition experiments against ancestral types that are often difficult to interpret and challenging to conduct. Observation of the genealogies of lineages as shown in Figure 3 led to realisation that the probability of avoiding extinction is a good predictor of future evolutionary success. Henceforth, measures of fitness were determined, not by competition with an ancestral type, but by measuring the number of lineage extinction events after replicate lineages of single test genotypes have gone through a further life cycle generation.

New experiments were conducted with the same protocol as for the main lineage-selection experiment and performed for a single cycle, each time starting with a population of eight microcosms founded by the same genotype. At the end of phase I, the presence of a mat was recorded and the density of SM cells was measured though plating. At the end of phase II, the density of WS cells was estimated through plating.

This experiment was conducted a total of x times for different genotypes. For each genotype, we estimated the probability of three events: M the production a mat at the end of phase I, S_I the production of cells with the switched phenotype SM cells at the end of Ph I, S_{II} the production cells with the switched phenotype WS at the end of Ph II. Further, we defined the "fitness" of a genotype as its probability to survive a full two-phase cycle, as the probability to survive both phases, hence $F = \mathbf{P}(M \wedge S_I \wedge S_{II})$.

We estimated the three probabilities by maximum of likelihood on a beta-binomial model, with a non informative prior (uniform in [0,1]). As a consequence, ff there were n independent trails and k successes, the estimate of probability is simply the proportion of successes $\hat{p} = k/n$, and the Bayesian confidence interval is given by the quantiles of a beta distribution parametrised as Beta$(1+k, 1+n-k)$.

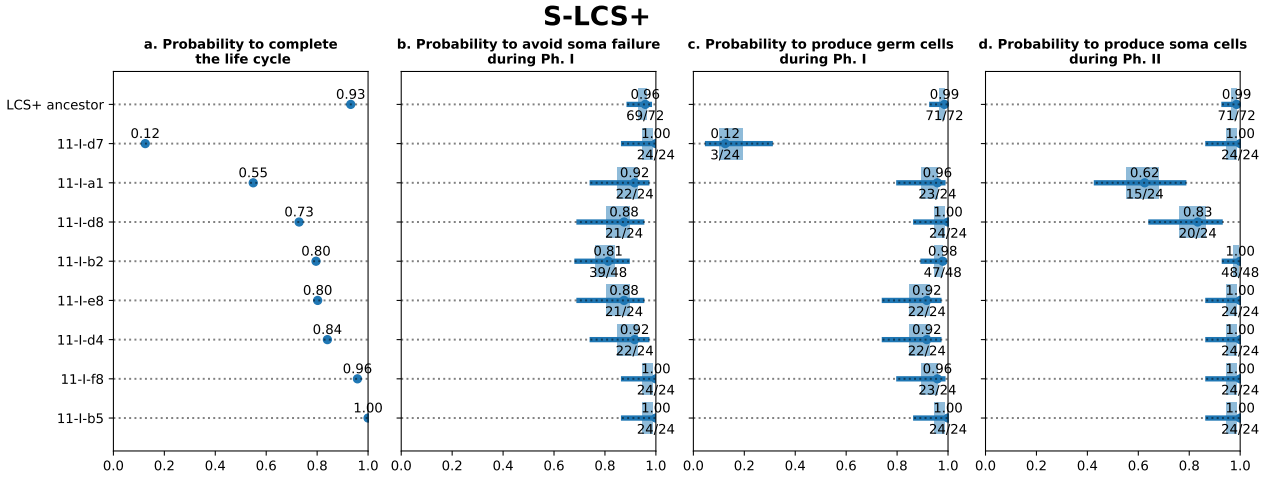

Figure S17. Probabilities in S-LCS+ endpoints. Same caption than Figure 7

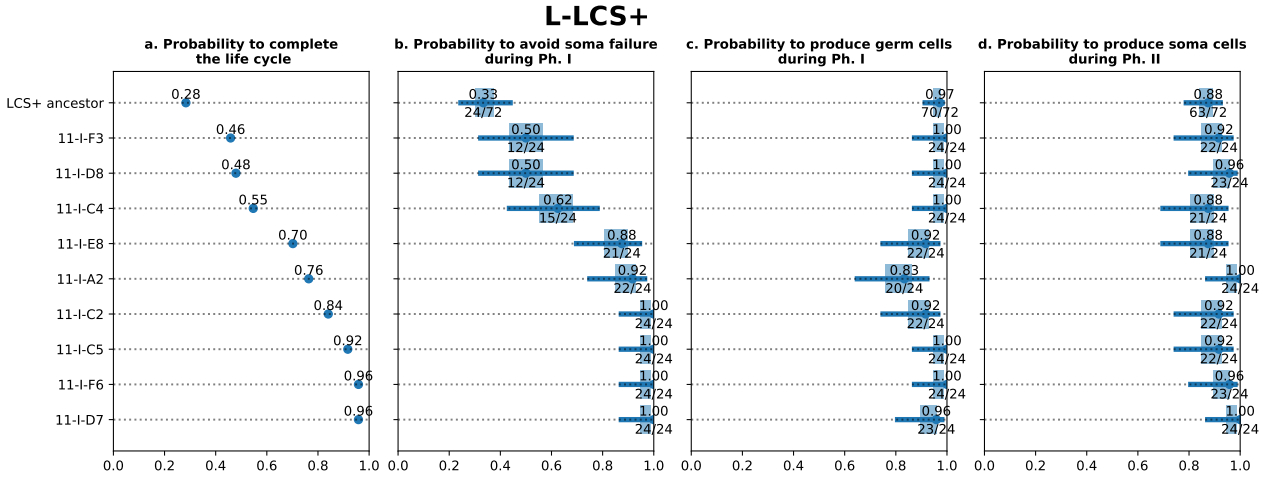

Figure S18. Probabilities in L-LCS+ endpoints. Same caption than Figure 7

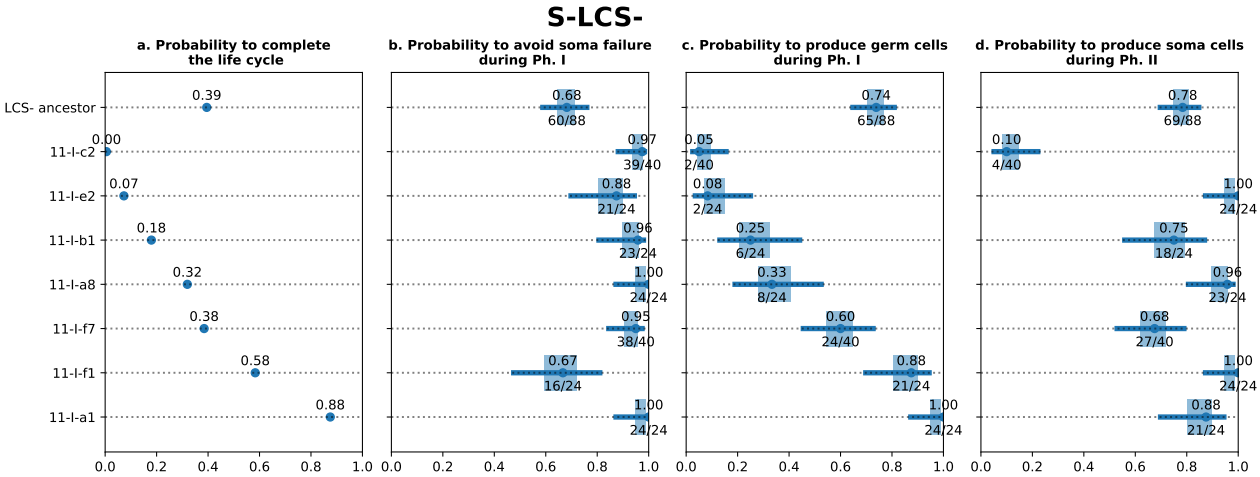

Figure S19. Probabilities in S-LCS- endpoints. Same caption than Figure 7

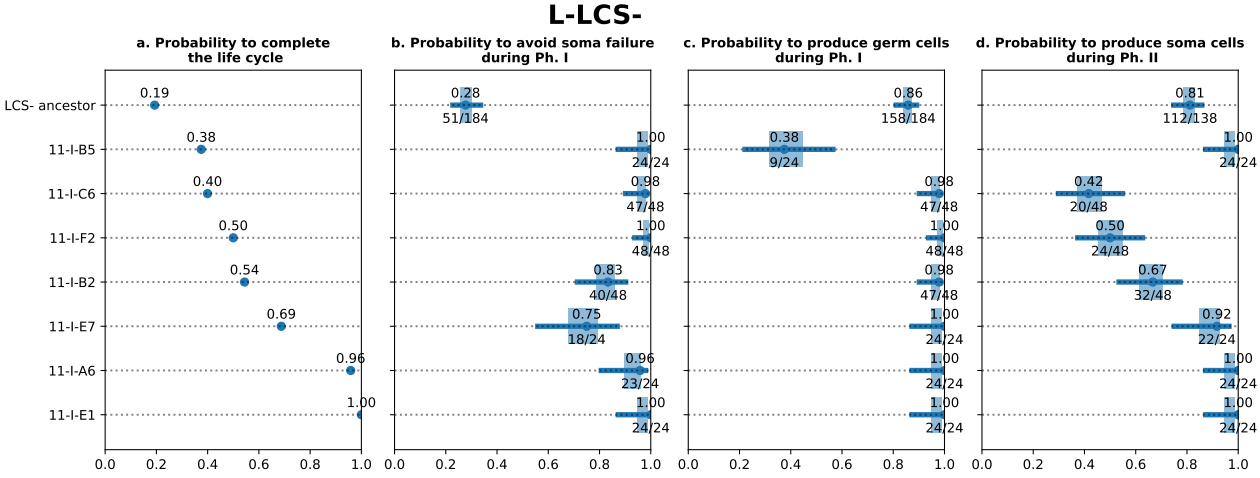

Figure S20. Probabilities in L-LCS- endpoints. Same caption than Figure 7

References.

Dempster, A. P., Laird, N. M., and Rubin, D. B. (1977). Maximum Likelihood from Incomplete Data via the EM Algorithm. *Journal of the Royal Statistical Society. Series B (Methodological)*, 39(1):1–38.

Efron, B. (2013). Bayes' Theorem in the 21st Century. *Science*, 340(6137):1177–1178.

Hammerschmidt, K., Rose, C. J., Kerr, B., and Rainey, P. B. (2014). Life cycles, fitness decoupling and the evolution of multicellularity. *Nature*, 515(7525):75–79.

Koller, D. and Friedman, N. (2009). *Probabilistic graphical models: principles and techniques.* MIT press.

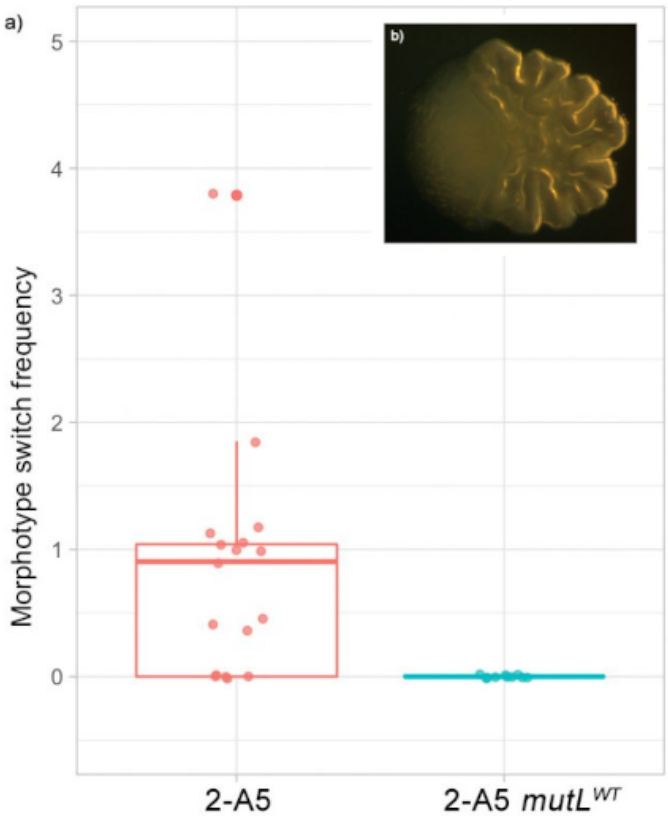

Figure S21. Colony morphology in 2-A5 Frequency of sectored colonies on plates (100-300 CFUs, 48h incubation) with switching *mutL* (L103R) morphotype in 2-A5 and 2-A5 with reconstituted *mutL* a); representative example of sectored colony showing morphotypic switch b).